ISSN 0280-5316
ISRN LUTFD2/TFRT--5775--SE

Modeling and Control of a 1.45 m deformable mirror

Pontus Giselsson

Department of Automatic Control
Lund University
October 2006

Department of Automatic Control
Lund Institute of Technology
Box 118
SE-221 00 Lund Sweden

Document name
MASTER THESIS

Date of issue
October 2006

Document Number
ISRN LUTFD/TFRT--5775--SE

Author(s)
Pontus Giselsson

Supervisor
Anders Rantzer at Automatic Control, and Torben Andersen at Lund Observatory in Lund.

Sponsoring organization

Title and subtitle
Modeling and Control of a 1.45 m deformable mirror (Modellering och reglering av en 1.45 m deformerbar spegel)

Abstract
The eagerness among astronomers to gain deeper knowledge and further understanding of the universe around us sets requirements for future telescopes.Images of more distant stars with higher spatial resolution is desired. Extremely Large Telescopes (ELTs) are being developed for this purpose. An example is a European collaboration that is developing an ELT called the Euro50. To obtain the desired resolution, disturbances that affect the incoming light need to be compensated for. This compensation is achieved by a constant reshaping of the secondary mirror in the telescope. The mirror reshaping is performed by force actuators that need to be controlled at a high bandwidth. The purpose of this Master Thesis is to derive a control law for a 1.45 m deformable mirror. The control strategy for this control law should be applicable and implementable in the secondary mirror of Euro50. The proposed control system strategy consists of actuator state feedback controllers of PD type and local observers that estimate the required states for the feedback.
This Master Thesis has been made in a joint collaboration between Lund Observatory at Lund University and the Department of Automatic Control at Lund Institute of Technology.

Keywords

Classification system and/or index terms (if any)

Supplementary bibliographical information

ISSN and key title
0280-5316

ISBN

Language
English

Number of pages
56

Recipient's notes

Security classification

Acknowledgements

I would like to thank my supervisors, Anders Rantzer at Department of Automatic Control, LTH and Torben Andersen at Lund Observatory, Lund University for their support and help during the project. I also want to send gratitude to my wife Michaela for being encouraging and supportive.

Contents

Chapter 1

Introduction

1.1 Extremely Large Telescopes - ELT

During the past few years a number of telescopes with apertures of up to 10 meters, Very Large Telescopes (VLT:s), have been constructed. Scientific observations and conclusions made from data received at these VLT:s, have been exciting for astronomers. Among other things the observations concerned studies of the early universe and its evolution, very distant galaxies and intergalactic matter. Astronomers however are facing challenges that require observations with even higher spatial resolution as well as more powerful light collection. In order to acquire these observations, Extremely Large Telescopes (ELT:s) are being developed.

1.2 Euro50 - Design

There is a European collaboration between scientists in five different countries doing technological studies on ELT:s. Their project is called Euro50[1]. A picture showing the suggested design of Euro50 is found in figure 1.1. It is decided for the Euro50 to have a two mirror design with one primary and one secondary mirror. The primary mirror is the light collector whereas the secondary mirror focuses the light for observations to be possible. The name Extremely Large Telescopes originates in the fact that their primary mirrors are large, in this case 50 meters. It would be inappropriate to use a monolithic mirror as primary mirror for several reasons. There are manufacturing problems as well as problems with transport, when dealing with such large apertures. Further it would be expensive to reproduce if a misfortune happens during handling or manufacturing. Therefore a segmented primary mirror with 618 segments, where each segment is 2 meters wide, is planned. The full primary mirror, as

[1]Read more about Euro50 and its design in [7]

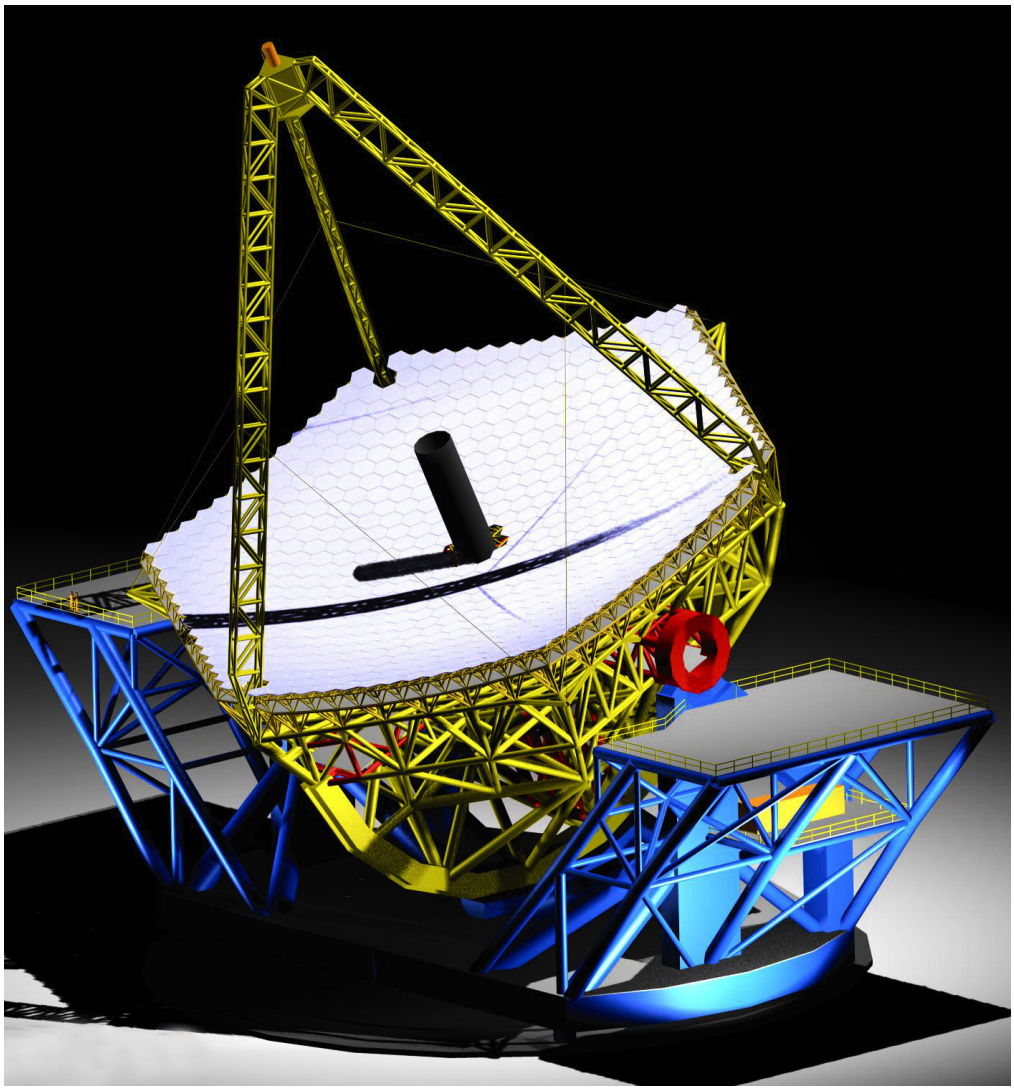

Figure 1.1: The suggested design of Euro50 with a segmented primary mirror and the secondary mirro in the tripod.

well as its segments, has a hexagonal shape. The shape of the primary mirror segments are controlled via a primary mirror alignment system that operates within a bandwidth of 10 Hz. Its purpose is to align the segments to form a monolithic-like surface and to correct for natural effect such as wind disturbances. Also the secondary mirror is hexagonal. It will be a monolithic deformable mirror that is slightly less than 4 meters in diameter.

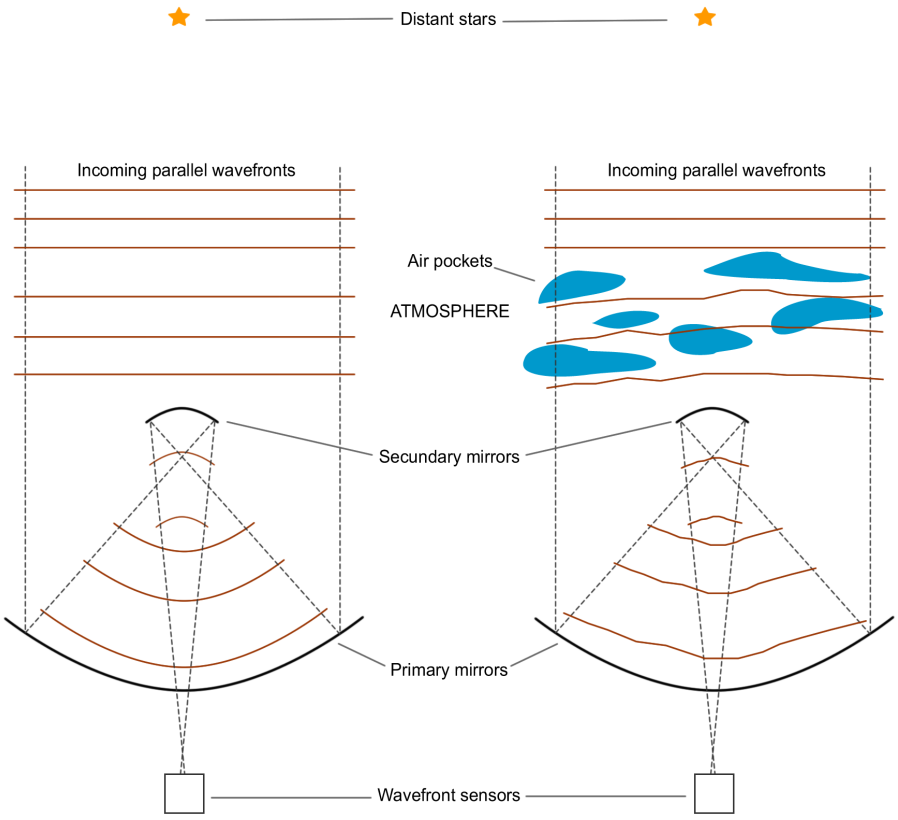

Figure 1.2: The left figure shows the case when no atmospheric distortion is present. The right figure shows how atmospheric distortion affects the incoming wavefronts. This distortion results blurry images of distant stars in the telescope.

1.3 Atmospheric distortion

As opposed to space telescopes as Hubble Space Telescope, Earth based telescopes such as ELT:s have atmospheric distortion to deal with. Because of uneven heating and cooling of the atmosphere, small pockets of air and water vapor that move around are created. These small pockets act like little lenses since their refractive indices differ. Parallel light rays, originating from distant galaxies, do bend randomly when traveling through the atmosphere due to these pockets. This effect is called atmospheric distortion, which is graphically explained in figure 1.2. The light rays that are reflected by the primary mirror are not parallel. Therefore the light rays will be focused to slightly differing points instead of at one focal point. This slightly defocused light will lead to blurry images of distant stars. In the figure the incoming light is represented as wavefronts instead of light rays. The atmospheric distortion has

to be compensated for in order to achieve desirable resolution for Euro50 and other ELT:s. A control system, usually referred to as adaptive optics, must be developed to compensate for the distortion.

1.4 Adaptive optics

The idea behind adaptive optics is to reshape the secondary mirror surface with high frequency. The objective of the reshaping is to cancel the effect of atmospheric distortion. This is done through making the reflected wavefronts parallel. This will result in pictures with a higher resolution. To be able to shape the deformable mirror, force actuators mounted at the back of the mirror is used. In order for a closed loop control law to be implementable, also sensors are mounted at the back of the mirror.

The control system need reference signals to know how to compensate for the distortions. These reference signals are retrieved by a matrix of Shack-Hartmann wavefront sensors[2] (WFSs) that analyzes the incoming light. The wavefront sensors are placed after the focal point of the secondary mirror. The conceptual design of a Shack-Hartmann WFS is shown in figure 1.3. In a Shack-Hartmann WFS the incoming light firstly passes though a lens that makes the light rays parallel. The parallel light rays then passes through many small lenses that are mounted in a matrix pattern. The small lenses focus the light to a certain point in the focal plane. If this point do not coincide with the focal point of the lens, the incoming light ray has been distorted. A CCD-camera then measures the deviation from the focal point of the little lenses. This gives information about how much the incoming light ray has been distorted. The incoming light can be represented as plane wavefronts with the same phase instead. The resulting wavefront is perpendicular to every light ray. This implies that wavefront slopes can be measured, instead of light ray angles, in accordance with the sensor name. All slopes of different parts of the wavefront can be interpolated in order to reconstruct a full wavefront. This reconstructed wavefront is mapped to reference signals for every actuator in the secondary mirror. The task for the adaptive optics control system is to follow this reference for every actuator.

1.5 Previous research

There is a couple of research groups involved in control of deformable mirrors. Among these, a group of Italian scientists from Osservatorio Astrofisico di Arcetri in Firenze, has been most successful so far. They have implemented

[2]Read about adaptive optics, atmospheric distortion and wavefront sensors in [11]

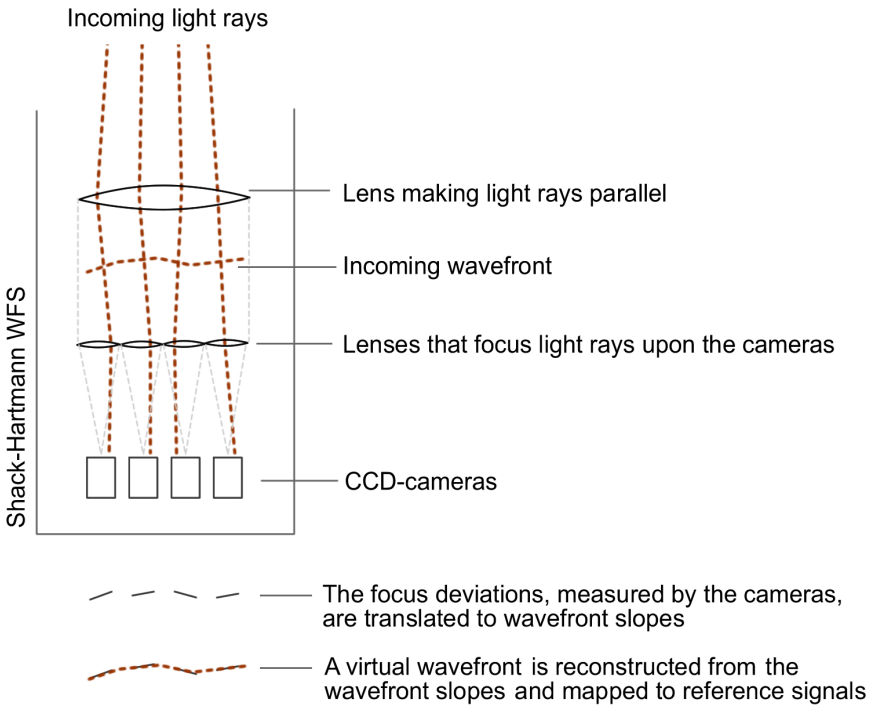

Figure 1.3: The figure shows the conceptual design of a Shack-Hartmann WFS.

control laws for two small physical deformable mirrors.

The first one is called MMT336[3] and is 64.2 cm in diameter. The number of actuators is 336. Collocated with every actuator there is a capacitive sensor that measures actuator deflection. They use equal proportional SISO controllers to control the different actuators. Since the material itself is poorly damped additional damping is needed to achieve good performance. A plate is mounted 50μm from the back of the mirror. The thin air gap between the mirror and the plate increases the mirror damping extensively, provided the air gap is small. The damping factor is inversely proportional to the gap size, h, to the power of three. Damping $\propto 1/h^3$. This results in a stable and fast controller. There are however disadvantages with this method. First of all the productional cost is high because of the required precision for the air gap. Furthermore the air gap is sensitive to dust, which can ruin the damping properties. Thus the Italian group abandoned this approach and introduced electronic damping instead.

[3]Read about the MMT336 in [4]

Their second mirror was called LBT672[4], with 672 actuators and a diameter of 91.1 cm. In this project the structural damping using a plate was abandoned and replaced by electronic damping. The electronic damping is straightforward. The sensor signals are differentiated, then sensor, and hence actuator, positions and velocities are known. Equal proportional-derivative (PD) controllers are implemented at every actuator location. The derivative part is used for damping purposes. This has shown to be a feasible and well performing approach when controlling a deformable mirror. To obtain accurate derivatives, sensor signals need to be low-pass filtered and sampled with a high frequency. The Italian group uses a position sampling frequency of 80 kHz.

The above mentioned adaptive mirrors are used or will be used in telescopes. The MMT336 is used in the Multiple Mirror Telescope situated on Mount Hopkins, Arizona. The other adaptive mirror, LBT672, will operate in the Large Binocular Telescope that is currently being constructed on a site at Mount Graham, Arizona[5].

[4]Read about the LBT672 in [5]

[5]Read about the MMT and the LBT telescopes in [2] resp. [1]

Chapter 2

Objective of this Master Thesis

Adaptive optics on large deformable mirrors has not yet been performed upon an actual mirror larger than 1 m. The vision of using adaptive optics with the secondary mirror of ELT:s, requires this to be possible. This Master Thesis is the first stage of an experiment that will take place at Lund Observatory. The objective of this experiment, hence also this Thesis, is to find a control law that controls a 1.45 m deformable circular mirror. This control law will then be expanded and applied to the secondary mirror of Euro50.

The control law will be derived under the following guiding principles.

1. The whole control system should be kept as simple as possible.
2. The objective is not to find an optimal controller, but to find a controller that is good enough.
3. Realization of the control system should be considered throughout the development process. The derived controller should be straightforward to implement in hardware and applied on the actual mirror.
4. Scalability of the control system is essential, in order to be applicable for the larger secondary mirror of Euro50.

2.1 Control system specifications

The specifications of the control system are determined by atmospheric aberrations and telescope vibrations. Euro50 will be developed to compensate for atmospheric aberrations in infrared (IR) wavelengths. The actuators, that control the mirror surface, should be mounted 68 mm from each other for IR compensation to be achieved. For the secondary mirror of Euro50, this leads to 3169 actuators, while the deformable mirror in this master thesis will have 420

actuators. Their stroke capacity is required to be up to 20 μm to compensate for atmospheric distortions as well as structural deflections that arise when the telescope is exposed to wind loads etc. These external disturbances will however be compensated by other control systems as well. The actuators will be controlled in closed loop, which requires sensor measurements. To minimize production costs, the sensors will not be collocated with the actuators. Sensors that are located at actuator locations require much higher manufacturing as well as mounting precision, which is expensive. Hence that configuration is not chosen for the Euro50 secondary mirror. The sensors and actuators are mounted in a hexagonal pattern at the back of the secondary mirror. This mounting pattern is used for the smaller circular mirror in this thesis as well, as shown in figure 2.1. As seen in the figure, there is a hole in the center of the mirror. The mirror will be fixed there and the outer edge will be unconstrained. The bandwidth requirement for the adaptive optics system is from 500 Hz up to 1 kHz to achieve satisfying compensation. Another performance criterion for the control system concerns the maximum Root Mean Square (RMS) value of deformation deviations. The RMS for the current configuration, where IR light is to be compensated for, is 80 nm. The RMS value is defined by

$$\sigma = \sqrt{\frac{1}{N}\sum_{k=1}^{N}\delta_k^2} \tag{2.1}$$

where N is the number of samples and δ is the deformation deviation.

2.2 Work procedure

First of all a model of the system will be created. The most common modeling strategy when dealing with structures is FEM-modeling. Femlab is used for as FEM-modeling software in this Master Thesis. Then a simulation environment will be set up in Simulink. Simulink is a tool for modeling and simulating different systems. It runs as a companion to Matlab, which is a widely used program for numeric mathematics. No actual mirror is available at this stage, so the derived control law will be tested upon a mirror model in Simulink. Controller stability and performance will be evaluated using Matlab and Simulink. Then the control law will be changed according to observations done during simulations. In a continuation of this Master Thesis the control law will be implemented in hardware and tested upon an actual mirror.

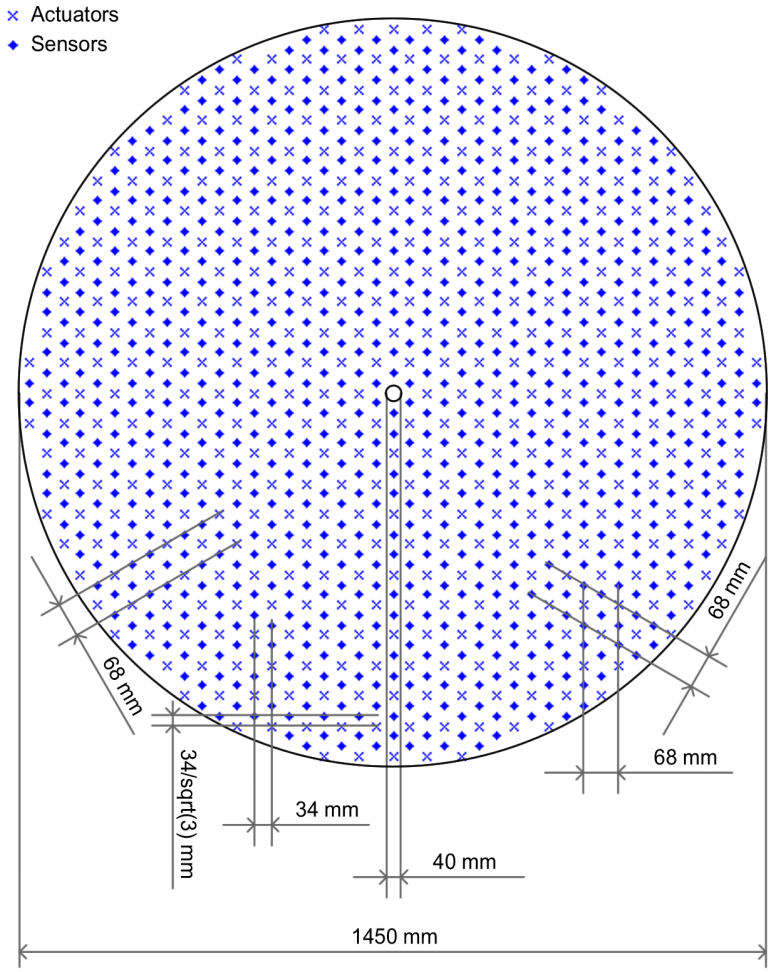

Figure 2.1: This is the layout of the deformable mirror in this Master Thesis. The crosses (x) denote actuator positions whereas the dots (.) denote sensor positions. There are altogether 420 actuators and 804 sensors.

Chapter 3

FEM-Modeling

In order to test a control law for the deformable mirror, a model of the mirror is needed. The most common modeling strategy for large mechanical structures is Finite Element Modeling, FEM. It is essential that this model is accurate enough for the controller to work with the actual mirror.

3.1 FEM-modeling

The idea of FEM-modeling[1] is to spatially discretize a structural system and to virtually interconnect neighboring discretization points, nodes, via springs and dampers. Every node has 6 degrees of freedom, dof:s, describing its possible movements. Three dof:s are translational whereas the other three are rotational dof:s. Actually it is the interaction between neighboring dof:s that is described with virtual springs and dampers. When connecting neighboring nodes with lines, a pattern called mesh is generated. The denser this mesh is, the closer to each other the nodes are and the more accurate the model gets. To achieve acceptable performance of the model a large number of nodes have to be chosen. This in turn makes the number of dof:s large. Since the interaction between neighboring dof:s is represented by springs and dampers, the interaction is mathematically described by spring-equations. The resulting equation-system that appears when assembling all these equations into matrices is usually very large. A feature of the system matrices is that they are sparse since the dof:s are connected only to their neighbors. The equation-system that describes the physical system is:

$$M\ddot{x} + C\dot{x} + Kx = F \tag{3.1}$$

M is the mass matrix, C the damping matrix and K the stiffness matrix. The F vector represents the force load acting upon the different dof:s. The system

[1] Read more about FEM-modeling in [9] and [8].

can be described in state space coordinates. Choosing positions and velocities as states, the equation-system becomes:

$$\begin{pmatrix} \dot{x} \\ \ddot{x} \end{pmatrix} = \begin{pmatrix} 0 & I \\ -M^{-1}K & -M^{-1}C \end{pmatrix} \begin{pmatrix} x \\ \dot{x} \end{pmatrix} + \begin{pmatrix} 0 \\ M^{-1} \end{pmatrix} F \tag{3.2}$$

3.2 Model reduction techniques

Since FEM-modeling usually generates large system matrices, computer simulations using them are cumbersome. To reduce simulation times and to prevent memory allocation errors, model reductions are of great need. The following sections will describe some useful methods that reduce the number of states which in turn decreases the computational burden when simulating.

3.2.1 Modal truncation

Modal truncation[2] is a commonly used reduction method. The idea is to describe the system with the modes that are significant to the behavior of the structure. The rest of the modes are truncated since their influence upon the total behavior is negligible. A great benefit of this method is that it diagonalizes the system matrices. This leaves a decoupled system, saying that the modes do not influence each other. Modal truncation on a FEM-model generates a system that is described by a number of uncoupled second order differential equations. A difficulty might be to choose the important modes. There are different methods that apply to different systems. One approach is to choose a sufficient number of the lowest frequency modes. More reliable methods involve calculation of the importance of each mode according to different norms. When truncating the system, the chosen eigenmodes are put in columns in a matrix, Φ. The eigenmodes are calculated from the generalized eigenvalue problem $K\Phi = M\Phi\Lambda$. Changing coordinates in 3.1 from $x = \Phi q$ and left multiplying with Φ^T gives:

$$\Phi^T M\Phi\ddot{q} + \Phi^T C\Phi\dot{q} + \Phi^T K\Phi q = \Phi^T F \tag{3.3}$$

Since the modes are shape functions they can be scaled by a factor and still be modes to the system. This implies that a normalization of the eigenmodes can take place. Mass normalization, $\Phi^T M\Phi = I$ is used to scale the modes. The stiffness matrix then becomes $\Phi^T K\Phi = \Phi^T M\Phi\Lambda = I\Lambda$, where Λ is a diagonal matrix containing the eigenvalues of the system. The damping matrix can be chosen to introduce ordinary second order systems for every modal coordinate, that is $\Phi^T C\Phi = 2Z\Lambda^{1/2}$ where Z contains the modal damping in

[2]Read more about modal truncation in [10].

a diagonal matrix. The eigenvalue matrix, Λ, equals Ω^2 where Ω is a diagonal matrix that contains the angular eigenfrequencies. This results in a system with a number of decoupled second order differential equations:

$$\ddot{q} + 2Z\Omega\dot{q} + \Omega^2 q = \Phi^T F \tag{3.4}$$

This shows that the system is diagonalized by the modal truncation. The eigenfrequencies of the system are obtained by dividing the angular eigenfrequencies, Ω, by 2π.

3.2.2 Guyan reduction

Another method that reduces the number of dof:s in a FEM-model is the Guyan reduction. The advantage of this method in comparison with the modal truncation is that Guyan reduction keeps a reduced number of the original dof:s which is useful in some applications. Also in Guyan reduction the retained dof:s has to be chosen. The retained dof:s are called master whereas the truncates ones are called slave. Methods that select optimal choices of master dof:s do exist. This is done by determining the ratio between stiffness and mass. High stiffness and low inertia gives a less significant dof and vice versa. All applications however do not require an optimal optimal choice of master dof:s. In these cases the master dof:s can be chosen arbitrarily. Accuracy of the reduced model then has to be tested. In Guyan reduction the mass- and stiffness matrices are rearranged according to master and slave dof:s:

$$\begin{pmatrix} M_{mm} & M_{ms} \\ 0 & 0 \end{pmatrix} \begin{pmatrix} \ddot{x}_m \\ \ddot{x}_s \end{pmatrix} + \begin{pmatrix} K_{mm} & K_{ms} \\ K_{sm} & K_{ss} \end{pmatrix} \begin{pmatrix} x_m \\ x_s \end{pmatrix} = \begin{pmatrix} F \\ 0 \end{pmatrix} \tag{3.5}$$

The inertia of the slave dof:s are approximated to be zero. The second row in the equation says $K_{sm}x_m + K_{ss}x_s = 0$ which is equivalent to $x_s = -K_{ss}^{-1}K_{sm}x_m$. A transformation matrix can be constructed:

$$\begin{pmatrix} x_m \\ x_s \end{pmatrix} = Tx_m \ , \ T = \begin{pmatrix} I \\ -K_{ss}^{-1}K_{sm} \end{pmatrix} \tag{3.6}$$

Changing coordinates and multiplying T^T from the left gives

$$M_r\ddot{x}_m + C_r\dot{x}_m + K_r x_m = F \tag{3.7}$$

where $M_r = T^T M T$, $C_r = T^T C T$, $K_r = T^T K T$ and $T^T(F\ 0)^T = F$.

These new mass and stiffness matrices are of the same size as the number of dof:s retained. One approximation in this reduction method is that the mass elements associated with the slave dof:s are approximated to be zero. This is perhaps not a very good approximation, but the method is still very commonly used in FEM-modeling.

3.2.3 Dynamic condensation

The approximation of zero mass inertia for slave dof:s in Guyan reduction might be bad. Dynamic condensation is another reduction method that include the influence of the slave dof:s inertia. The method is very similar to Guyan reduction:

$$\begin{pmatrix} M_{mm} & M_{ms} \\ M_{sm} & M_{ss} \end{pmatrix} \begin{pmatrix} \ddot{x}_m \\ \ddot{x}_s \end{pmatrix} + \begin{pmatrix} K_{mm} & K_{ms} \\ K_{sm} & K_{ss} \end{pmatrix} \begin{pmatrix} x_m \\ x_s \end{pmatrix} = \begin{pmatrix} F \\ 0 \end{pmatrix} \tag{3.8}$$

The second row is extracted and transformed into the frequency plane. $-\omega^2 M_{sm} x_m - \omega^2 M_{ss} x_s + K_{sm} x_m + K_{ss} x_s = 0$ From this, the transformation matrix, T, can be derived:

$$\begin{pmatrix} x_m \\ x_s \end{pmatrix} = T x_m \ , \ T = \begin{pmatrix} I \\ -\left(K_{ss} - \omega^2 M_{ss}\right)^{-1} \left(K_{sm} - \omega^2 M_{sm}\right) \end{pmatrix} \tag{3.9}$$

The transformation matrix is applied in the same manner as in equation 3.7. Dynamic condensation optimizes the reduced systems accuracy at one desired frequency chosen in ω as opposed to Guyan reduction which optimizes accuracy in static conditions.

3.2.4 Iterative Improved Reduced System - IIRS

Iterative IRS is based on dynamic condensation and is extended with an additional corrective term that is generated iteratively. There are proofs, see [6], showing that the natural frequencies of the IIRS reduced model converge to the natural frequencies of the full model. Also for IIRS a transformation matrix is used to decrease the number of dofs. This transformation matrix, T_{i+1} applied in the same manner as in 3.9, is calculated and iteratively improved with the following formulas:

$$T_{i+1} = \begin{bmatrix} I \\ t_{i+1} \end{bmatrix} \tag{3.10}$$

where,

$$t_{i+1} = t_s + K_{ss}^{-1} [M_{sm} \ M_{ss}] T_i M_{Ri}^{-1} K_{Ri} \tag{3.11}$$

with,

$$t_0 = t_s = -K_{ss}^{-1} K_{sm} \tag{3.12}$$

The reduced stiffness and mass matrices after the i:th iteration are defined as:

$$K_{Ri} = T_i^T K T_i \tag{3.13}$$

and

$$M_{Ri} = T_i^T M T_i \tag{3.14}$$

This reduction method is more accurate than the two previously discussed. It requires however more computational effort to derive the desired model.

3.3 The mirror model

In this Master Thesis Femlab was used to create the desired FEM-model. Since the mirror is very thin compared to the diameter, 3.3 mm contra 1.45 m, it was modeled as a 2-D shell element. Shell elements describe the behavior better than 3-D elements when dealing with such ratios between dimensions. 3-D structures can shear lock themselves leading to smaller deflections in the model than in reality. Another advantage with 2-D shell elements is that the number of nodes is greatly reduced. Since structure behavior is known at node locations, actuator and sensor locations will be chosen as nodes. More nodes are necessary to describe the circular boundaries accurately. These extra nodes are automatically chosen by Femlab using Delaunay triangulation. The method maximizes the minimum angle of the triangles that appear when connecting the neighboring nodes with lines. This pattern is, as mentioned earlier, called a mesh and the density of this mesh is user defined in Femlab. Figure 3.1 does show the mesh and the interconnecting virtual springs and dampers for one chosen mesh density. The FEM-model equation has one mass matrix, one damping matrix and one stiffness matrix. The damping matrix can not be exported or predicted by a FEM-modeling program. Hence the damping has to be decided upon by the user. In cases of structures like this, a low modal damping is commonly used.

3.3.1 FEM-model verification

As mentioned the mesh density of the FEM-discretization is user defined. In Femlab there are seven different choices from extremely coarse, over normal to extremely fine. The accuracy of the different mesh choices can be analyzed. Analytical formulas for edge deflection when different loads are applied can be found in [12]. In chapter 10, table 24.1.l, an example that can be applied to this system is found. It is a circular, thin plate with fixed inner edge and a circular line load applied at a chosen radius from the center. The deflection at the outer edge is:

$$z = \frac{-wa^3}{D}\left[\frac{C_2}{C_8}\left(\frac{r_0 C_9}{b} - L_9\right) - \frac{r_0 C_3}{b} + L_3\right] \tag{3.15}$$

Where w is the line load [pounds/inch], a is the outer radius [inch], b the inner radius [inch], $D = Et^3/12(1-\nu^2)$, E is modulus of elasticity [pounds per square inch], ν is Poissons ratio, t is the plate thickness [inch], r_0 is the radius of the applied load, and the remaining constants are defined below:

$$\begin{aligned} C_2 &= (1/4)[1-(b/a)^2(1+2\ ln(a/b))] \\ C_8 &= (1/2)[1+\nu+(1-\nu)(b/a)^2] \end{aligned}$$

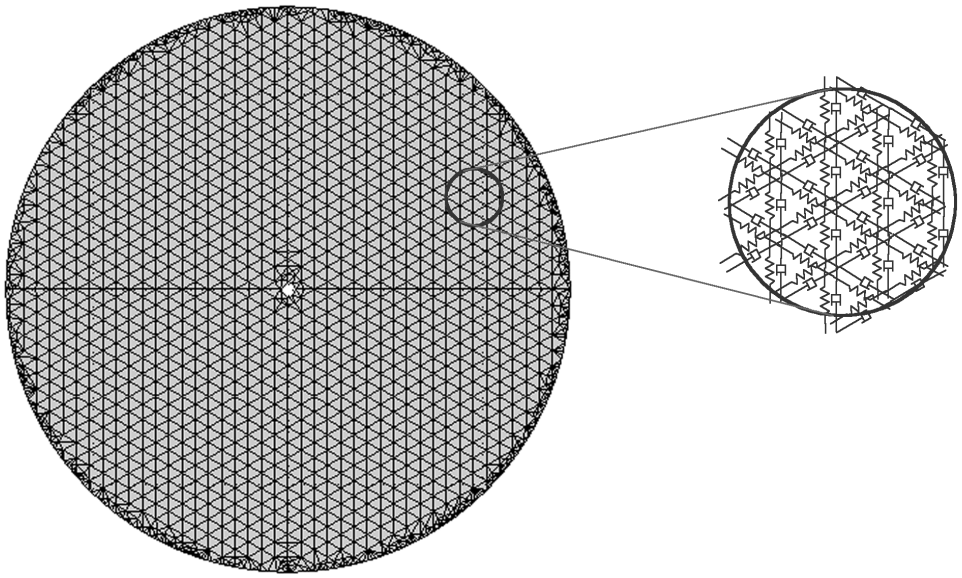

Figure 3.1: The left figure shows a mesh for the deformable mirror. Compare the mesh to sensor and actuator placements in 2.1. Every sensor and actuator position is a node in the mesh. The right figure shows how the nodes are virtually interconnected via springs and dampers in FEM-modeling.

$$
\begin{aligned}
C_9 &= (b/a)\{[(1+\nu)/2]\ ln(a/b) + [(1-\nu)/4][1-(b/a)^2]\} \\
C_3 &= (b/4a)\{[(b/a)^2+1]\ ln(a/b) + (b/a)^2 - 1\} \\
L_3 &= (r_0/4a)\{[(r_0/a)^2+1]\ ln(a/r_0) + (r_0/a)^2 - 1\} \\
L_9 &= (r_0/a)\{[(1+\nu)/2]\ ln(a/r_0) + [(1-\nu)/4][1-(r_0/a)^2]\}
\end{aligned}
$$

When applying a line load of 1.0 kg/m (= 0.0560 pounds/inch) at a 30.0 cm (= 11.811 inch) radius from the center the outer radius deflection according to the analytical formula is -70.498 μm. A comparison with deflections using different mesh densities in the FEM-model is done and presented below.

Mesh	**Nbr dof:s**	**Boundary deflection**	**Error**
Extremely coarse	11562	-71.93 μm	2.03 %
Coarser	18894	-71.10 μm	0.85 %
Normal	24300	-70.63 μm	0.19 %
Finer	26274	-70.58 μm	0.12 %
Extremely fine	38250	-70.53 μm	0.05 %

As seen, all different choices of mesh density lead to static errors less than approximately 2%. Since computer simulations on an ordinary PC are not feasible with any of the full FEM-models, model reductions are needed. These reductions introduce further approximations leading to errors. Hence the model

using the extremely coarse mesh density is sufficient and therefore chosen. It is preferable to keep the model as small as possible without compromising with its accuracy.

3.3.2 Selection and verification of reduced model

Different model reduction techniques are suitable for different problems. When a direct physical interpretation of the model states is desired, Guyan reduction, dynamic condensation or IIRS is appropriate. Modal truncation is commonly used when the states do not need to be physically observed. Another advantage with modal truncation is that a modal damping that is commonly used is easily implemented. Hence modal truncation is chosen to describe the mirror behavior when simulating.

As mentioned, the damping is not given by the FEM-program, leaving the decision of the damping matrix to the user. Modal damping is commonly accepted when dealing with structures like this mirror. Either a constant modal damping or a frequency dependent damping (Rayleigh damping), where higher frequency modes are more damped, is usually chosen. In this thesis both low constant modal damping and low frequency dependent damping is evaluated. Figure 3.2 plots Bode diagram for all actuator to actuator transfer functions with a constant modal damping of 0.02. The figure contains only 43 different Bode plots. All actuator to actuator transfer functions are there since there is symmetry in actuator placements leading to some identical transfer functions.

Modal truncation says that modes are to be truncated from the mirror model. The retained modes have to be chosen somehow as discussed in 3.2.1. Here the one thousand lowest frequency eigenmodes are retained and the rest are truncated. The frequencies of the retained modes range from 3.8 Hz up to 5504 Hz. Sufficiency in the number of retained modes must be verified. This is done through analysis of static behavior as well as a discussion about how the different modes will be controlled. Some of the mode shapes are shown in figure 3.3.

All the different modes have different stiffness. Low frequency modes have low stiffness and accordingly high frequency modes have high stiffness. This implies that different forces have to be applied to deflect different modes equally much. For the lowest frequency mode to deflect a maximum of 1 μm a 5×10^{-4} N force is needed. In order to deflect mode 1000 a maximum of 1 μm a force of 1 kN is required. Applying 1 N to mode 30 results in 1 μm deflection. Since the control system will operate with forces around 1 N and mirror deflections around 1 μm only low order modes, approximately a couple of hundred, will

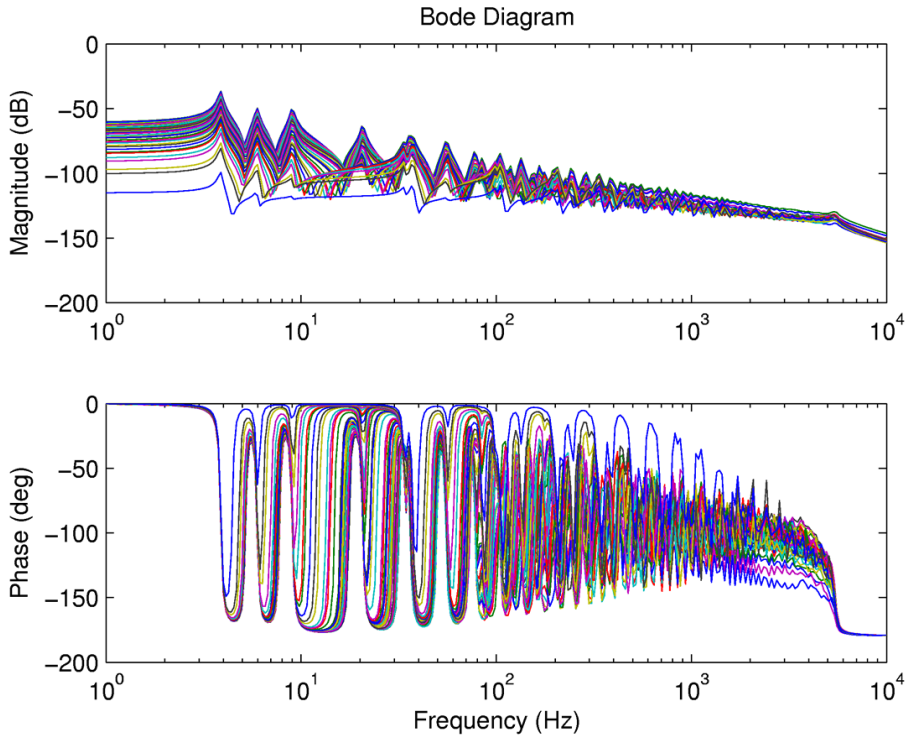

Figure 3.2: Bode diagrams for the different actuator to actuator transfer functions when having constant modal damping of 0.02 and the modal truncated model.

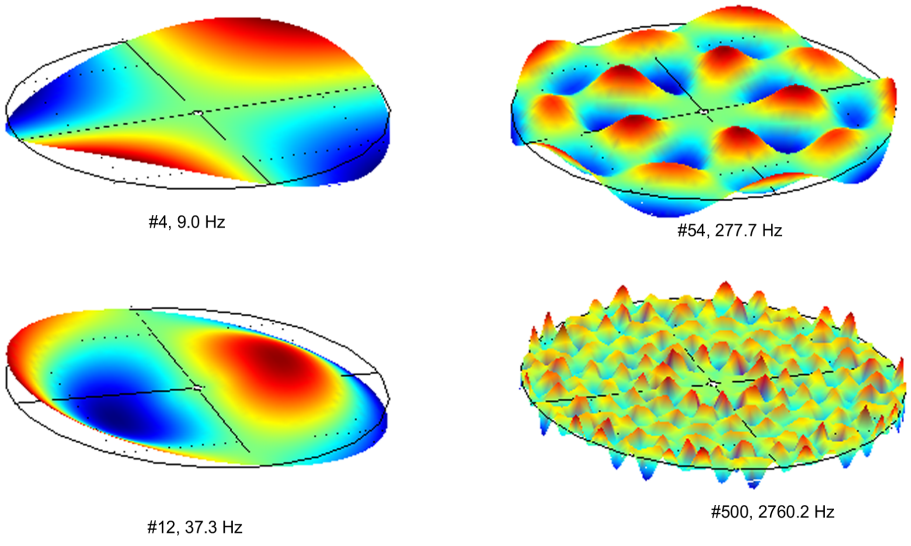

Figure 3.3: Some of the mirror eigenmodes are plotted in this figure. Mode number and eigenfrequency for each mode is also presented.

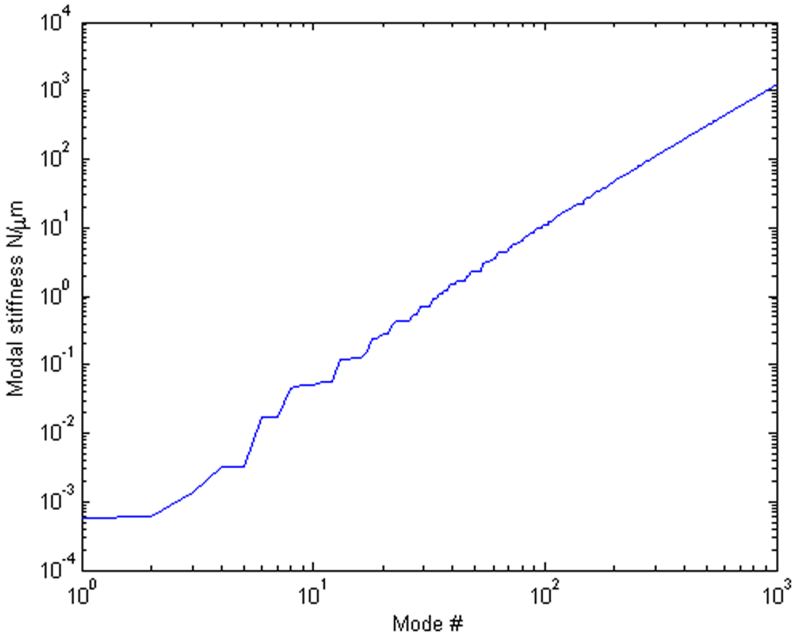

Figure 3.4: The figure shows the modal stiffness. Too stiff modes are not controlled in closed loop but in open loop via the feed forward.

be controlled in closed loop. Higher order modes are controlled in open loop using feed forward to achieve correct static behavior. This implies that a sufficient number of modes are retained to describe system behavior satisfactorily, if the static behavior is acceptable. Even higher order modes can be interpreted as noise to the system. A plot showing stiffness contra mode number is presented in figure 3.4.

Comparing the reduced model with the full FEM-model when applying a 1 N force at an actuator position lead to small differences. The largest ratio between the deflections of the reduced model and the full FEM-model appear close to the inner boundary. The ratio is however everywhere less than 1.0005 which confirms the correctness and accuracy of the derived reduced model.

Three more reduction methods have been described in this chapter. These are used to derive a model for actuator and sensor positions and velocities out of plane, since these are the interesting states when controlling the structure. The accuracy of the reduced models will be discussed here. The IIRS-reduced model has been derived by 25 iterations.

Among the 1000 retained modes in modal truncation, 23 are purely in-plane modes. The reduced models describe deflections out of plane; hence these 23 modes will not be contained in the reduced models. Taking this into consideration a modal frequency comparison can be made. As mentioned the lowest frequent modes are controlled through feedback, hence these are most important. Mean natural frequency errors in percentage for the different models are presented below:

	Guyan reduction	**Dynamic condensation**	**Iterative IRS**
Avg err, 1000 modes	35.2%	7.3%	0.08%
Avg err, 300 lowest modes	26.5%	0.8%	0.02%

This says that IIRS is the best reduction method dynamically. Statically all methods produce errors smaller than 0.001% when applying a 1 N force at an actuator location. The dynamic accuracy of the model is, however, more dependent upon the choice of damping matrix than the choice of reduction method. Hence dynamic condensation will be used when a direct physical interpretation of the states is needed in subsequent chapters. The dynamic condensation is accurate enough and it is much faster to obtain a reduced model using this method than with IIRS.

3.4 Simulation

The purpose of the mirror model and its reductions is to enable simulation of the mirror behavior. This renders information about how the mirror behaves when subjected to forces. In the previous section a modal truncated FEM model was decided upon to represent the mirror. The mirror model equations are (see 3.4):

$$\begin{aligned} \ddot{q} + 2Z\Omega\dot{q} + \Omega^2 q &= \Phi^T F \\ y &= Cq \end{aligned} \tag{3.16}$$

The state space representation of the system is:

$$\begin{aligned} \begin{pmatrix} \dot{q} \\ \ddot{q} \end{pmatrix} &= \begin{pmatrix} 0 & I \\ -\Omega^2 & -2Z\Omega \end{pmatrix} \begin{pmatrix} q \\ \dot{q} \end{pmatrix} + BF \\ y &= Cq \end{aligned} \tag{3.17}$$

where $B = (0 \ \Phi^T)^T$. Simulink is used to create the desired simulation environment. The Simulink representation of the modal mirror model is shown in figure 3.5. The routing in the model is optimized with respect to simulation times. Different control algorithms will be derived in subsequent chapters.

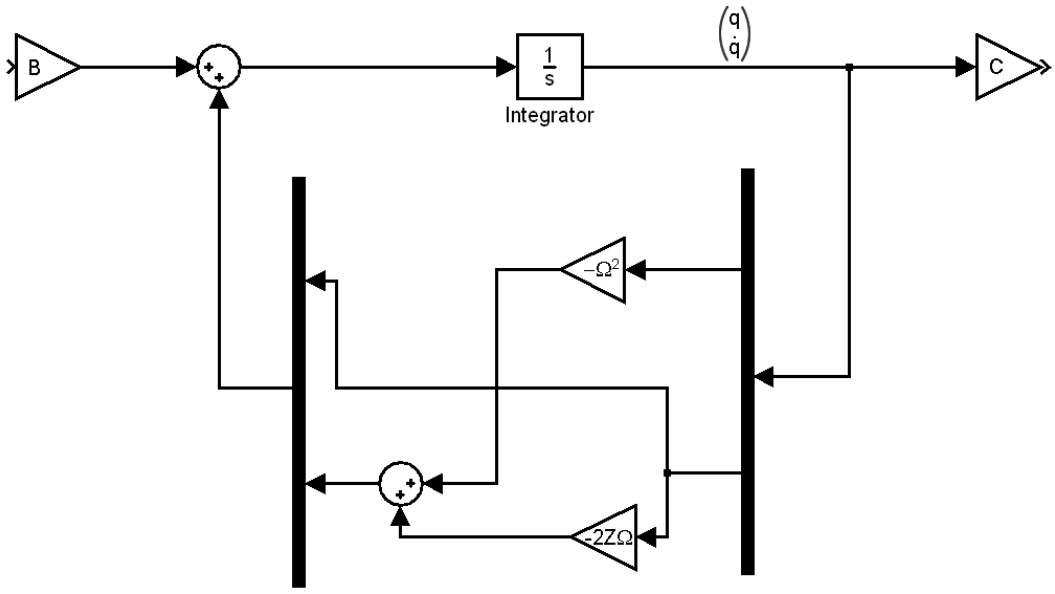

Figure 3.5: The Simulink model of the mirror. Compare the routing to the state space model in equation 3.17.

The performance of these algorithms will be tested in this simulation environment.

Chapter 4

Control

4.1 Control strategy

To decide upon a control strategy, previous research (section 1.5) is considered, bearing the guiding principles (chapter 2) in mind. The simplicity of the second SISO approach developed by the Italian group with PD controllers for every actuator is appealing. The difference between the mirror of the Italian group and the mirror in this master thesis is that the sensors are not collocated in this problem. This suggests a control law based on a state feedback controller with an observer that estimates actuator positions and velocities. The estimates will be fed back to the local SISO controllers that will be implemented as ordinary PD controllers. To benefit from the SISO controlling scalability, the observer needs to be distributed. To update a state in a distributed observer, only information from its physically neighboring states should be needed. A centralized observer, on the other hand, needs information from all states to update other states. When the system is large and complex, a distributed control approach implies faster and more efficient control. The poorly damped material, with many eigenfrequencies inside the desired controller bandwidth, requires a controller with high sampling frequency. Also this implies that a distributed controller is preferable. Preceding considerations imply that this control strategy can be divided into two subtasks:

1. Find a controller that stabilizes the mirror with actuator state-feedback, starting with a SISO approach.

2. Create a distributed observer that estimates position and velocity in the actuator positions.

4.2 State feedback control

As mentioned the control problem can be divided into two subtasks. In this chapter a state feedback controller will be designed. Information about actuator positions and velocities is assumed here assumed to be known.

4.2.1 SISO controller

The simplest distributed controller is to have a SISO controller for every actuator. These SISO controllers calculate the actuator forces with feedback from the same actuator states only. The force applied by an actuator is calculated by:

$$f = -n(x - x_r) - l\dot{x} + n_r x_r \tag{4.1}$$

where x = actuator position, $\dot{x}$ = actuator velocity, x_r = reference value, n = proportional gain, l = derivative gain n_r = feed forward gain. This is an ordinary PD controller that is used at all actuator locations. The proportional part and the derivative part control the actuator in closed loop. The feed forward is an open loop component that is added to eliminate static errors. When assembling all PD controllers into matrix form, the following system equation appear (compare to equation 3.1).

$$M\ddot{x} + C\dot{x} + Kx = -FNF^T(x - x_r) - FLF^T\dot{x} + FN_rF^T x_r \tag{4.2}$$

The F factor in FNF^T and FLF^T decides upon which state the applied actuator forces operate in the equation system. N and L are diagonal matrices since the controllers are chosen to be of SISO type. All the different SISO controllers are represented with their respective proportional gain, n in the diagonal of N. The same holds for L and l. Absolute tuning of these parameters is somewhat uninteresting since direct feedback from actuator states is impossible when dealing with the actual mirror. The diagonal elements of N, that is the proportional part of the PD controllers, are however chosen to create a not too large overshoot when executing a step response test. The diagonal elements of L, that is the derivative part of the PD controllers, are then chosen to minimize oscillations after a step response test. n and l for the different SISO controllers are chosen equal, since the interaction between neighboring actuators is large. Then the effect of neighboring control action is not too significant to compensate for. The feed forward term N_r is the only control parameter left to decide. The purpose of N_r is to eliminate static errors by making the static amplification one. Calculation of N_r is done by transforming the system into state space, $z = (x\ \dot{x})^T$:

$$\begin{pmatrix} \dot{x} \\ \ddot{x} \end{pmatrix} = A \begin{pmatrix} x \\ \dot{x} \end{pmatrix} + B \begin{pmatrix} x \\ \dot{x} \end{pmatrix} + Rx_r \tag{4.3}$$

$$y = (D \;\; 0)\begin{pmatrix} x \\ \dot{x} \end{pmatrix}$$

where,

$$\begin{aligned} A &= \begin{pmatrix} 0 & I \\ -M^{-1}K & -M^{-1}C \end{pmatrix} \\ B &= \begin{pmatrix} 0 & 0 \\ -M^{-1}FNF^T & -M^{-1}FLF^T \end{pmatrix} \\ R &= \begin{pmatrix} 0 \\ M^{-1}F(N_r+N)F^T \end{pmatrix} \end{aligned} \tag{4.4}$$

Hereafter the transfer function from reference signal to output is calculated:

$$Y(0) = (D \;\; 0)(sI - A - B)^{-1}(0 \;\; M^{-1}F(N+N_r)F^T)^T X_r \tag{4.5}$$

Statically the transfer function is $D(-A-B)^{-1}(0 \;\; M^{-1}F(N+N_r)F^T)^T$. N_r is chosen to make the static transfer function equal to the identity matrix, which eliminates static errors because $Y(0) = IX_r$. This feed forward matrix, N_r, is however dependent on the mirror model. If the static deflections of the model are not the same as those of the actual mirror, this feed forward matrix has to be adjusted. Further the feed forward term is centralized, meaning that all reference signals influence all actuators to achieve correct static behavior. This is not in contradiction to the stated control strategy of a fast distributed controller. The reason is that the references will be applied in a slower outer control loop. When dealing with the actual mirror, this feed forward matrix cannot be directly applied. It is sensitive to mounting errors etc and has to be determined once the mirror is at place.

This controller has in simulations shown good performance. Exact performance evaluation at this stage is however not interesting since this controller without observer is not realizable. Further it has been proved to be stable with all closed loop system eigenvalues in the left half plane. Mathematical considerations can also be used to prove stability which is done below. The feedback dynamics of system is:

$$M\ddot{x} + C\dot{x} + Kx = -FNF^T x - FLF^T \dot{x} \tag{4.6}$$

A Lyapunov function, $V(x)$, i chosen:

$$V(x, \dot{x}) = \dot{x}^T M \dot{x} + x^T (K + FNF^T)x \tag{4.7}$$

Differentiating $V(x, \dot{x})$ with respect to time gives:

$$\dot{V}(x, \dot{x}) = \dot{x}^T M \ddot{x} + \ddot{x}^T M \dot{x} + \dot{x}^T (K + FNF^T)x + x^T (K + FNF^T)\dot{x} \tag{4.8}$$

Since $M = M^T$ and $(K + FNF^T) = (K + FNF^T)^T$ the following hold:

$$\ddot{x}^T M\dot{x} = (\ddot{x}^T M\dot{x})^T = (M\dot{x})^T\ddot{x} = \dot{x}^T M\ddot{x} \tag{4.9}$$

and

$$x^T(K+FNF^T)\dot{x} = (x^T(K+FNF^T)\dot{x})^T = ((K+FNF^T)\dot{x})^T x = \dot{x}^T(K+FNF^T)x \tag{4.10}$$

Insertion of 4.9 and 4.10 into 4.8 gives:

$$\begin{aligned} \dot{V}(x,\dot{x}) &= 2\dot{x}^T M\ddot{x} + 2\dot{x}^T(K + FNF^T)x \\ &= 2\dot{x}^T(-(C + FLF^T)\dot{x} - (K + FNF^T)x) + 2\dot{x}^T(K + FNF^T)x \\ &= -2\dot{x}^T(C + FLF^T)\dot{x} \end{aligned} \tag{4.11}$$

Lyapunov theorem for global asymptotic stability says that if:

1. $V(0) = 0$
2. $V(x) > 0$ for all $x \neq 0$
3. $\dot{V}(x) < 0$ for all $x \neq 0$
4. $V(x) \to \infty$ as $\| x\| \to \infty$

then $x = 0$ is globally asymptotically stable. Since M, $K+FNF^T$ and $C+FLF^T$ are all positive definite, the Lyapunov conditions hold, which proves stability for this state feedback controller when fed with correct state information.

4.3 Simulation

When the feedback is assumed to be exactly correct, information about actuator states can be extracted from the mirror model when simulating. The simulation environment in Simulink is shown in figure 4.1. The mirror model is the same as in figure 3.5.

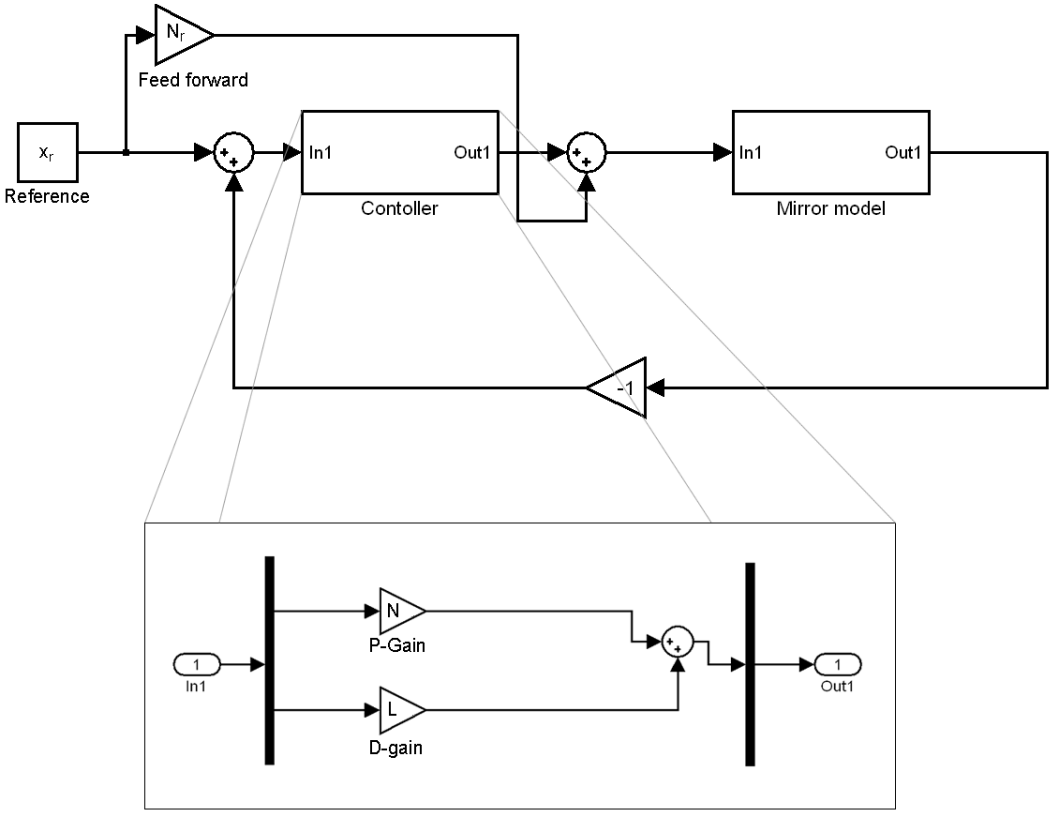

Figure 4.1: The Simulink model when the controller is fed with actual actuator state information. The states are position and velocity. N is the proportional gain of the controller and the L is the derivative gain of the controller. The subsystem ”Mirror model” is shown in figure 3.5.

Chapter 5

Observer

The derived controller requires accurate state feedback from actuator positions and velocities. Since the sensors are located between the actuators, sensor measurements cannot directly serve as state feedback. An observer is needed to estimate the actuator states. The overall control strategy is to have a fast local feedback; therefore the observer should be distributed. In this section different observers and their accuracy will be discussed in order to decide upon what kind of observer that is needed. The possibility to distribute the observer is crucial, this will be addressed ones an accurate enough central observer is obtained.

5.1 Smoothing

Initial attempts to find an observer was carried out using spatial smoothing. The idea behind smoothing is to retrieve the shape of a structure based on spatially discretized samples. In this case sensors are the discretized sampling points. The whole structure shape is not needed here, only actuator positions need to be known. Every actuator has six surrounding sensors. One smoothing possibility would be to create a mean value from the surrounding sensors and use it as position state for the actuator. This is however not accurate enough since the largest deformations appear in actuator locations where the forces are applied. Figure 5.1 illustrates the problem. In order to create a more accurate observer based on smoothing, a Guyan reduced model, 3.2.2, is used. The retained states are z-translations for actuators and sensors. The following matrix transformations are used to create a static relationship between sensor measurements and actuator states.

$$K_r x_m = \begin{pmatrix} K_{aa} & K_{as} \\ K_{sa} & K_{ss} \end{pmatrix} \begin{pmatrix} x_a \\ x_s \end{pmatrix} = \begin{pmatrix} F \\ 0 \end{pmatrix} \tag{5.1}$$

Index a is for actuators and s for sensors. Rearranging the second row of the matrix equality gives: $x_s = -K_{ss}^{-1} K_{sm} x_m$. Pseudo inverting the transformation

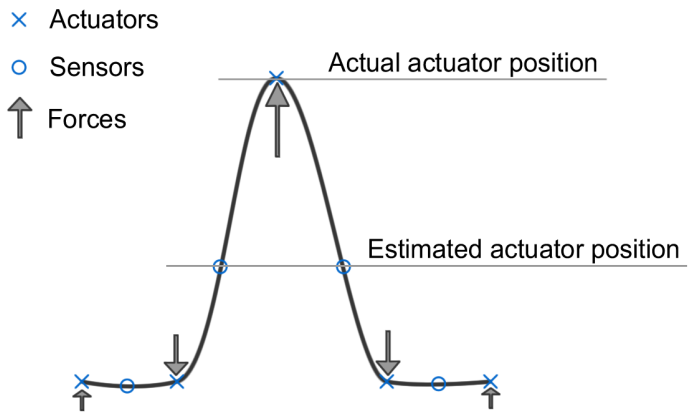

Figure 5.1: The figure shows why the mean value of surrounding sensor measurements is a bad estimation of the actuator position. This is because the maximum deformations appear where the forces are applied.

matrix $-K_{ss}^{-1}K_{sm}$ gives the static relationship between sensor and actuator positions.

5.1.1 Limitations

There are two main limitations when using smoothing in this context. It only estimates position states and no velocity states. To estimate velocities, a differentiation of position estimates has to take place. This would be possible if sensor signals were being low-pass filtered and sampled with a high frequency. The other limitation is of more important nature. Smoothing in this case considers only static relationships. Control of structures of this type requires dynamically as well as statically accurate estimates. Smoothing does not give accurate enough state estimates, hence this approach is abandoned.

5.2 Kalman filtering

Feedback requirements of dynamically and statically correct estimates suggest that a Kalman filter is needed. General Kalman filters will be briefly introduced before discussing Kalman filters in this particular case. The idea of the Kalman filter is to use a model of the structure whose states are to be estimated. In addition a corrective term is applied comparing the plants outputs to the Kalman filter outputs. The discrete Kalman filter:

$$\hat{x}(k+1) = \Phi\hat{x}(k) + \Gamma u(k) + K_d(y(k) - D\hat{x}(k)) \tag{5.2}$$

The continous Kalmanfilter:

$$\dot{\hat{x}} = A\hat{x} + Bu + K_c(y - D\hat{x}) \tag{5.3}$$

Comparison with the FEM state space model 3.2 shows that the difference is the additional corrective term, $K_c(y - D\hat{x})$. This term compares the observer output to the plant output. The K matrices are determined to minimize the estimation error variance using the continuous respective the discrete Riccati equations. The hat in the above equations denotes that it is an estimate of the real state. In this Thesis mostly discretized Kalman filters with high sampling frequencies will be used to reduce simulation times. The theory however will be mostly covered in continuous time since the original FEM-model is continuous.

5.2.1 Kalman filtering using the full FEM-model

Problems occur directly when trying to use the Kalman filter with the full FEM-model. A state space representation of the Kalman filter in this case is:

$$\begin{pmatrix} \dot{\hat{x}} \\ \ddot{\hat{x}} \end{pmatrix} = \begin{pmatrix} 0 & I \\ -M^{-1}K & -M^{-1}C \end{pmatrix} \begin{pmatrix} \hat{x} \\ \dot{\hat{x}} \end{pmatrix} + \begin{pmatrix} 0 \\ M^{-1} \end{pmatrix} F + K_c \left(y - (D\ 0) \begin{pmatrix} \hat{x} \\ \dot{\hat{x}} \end{pmatrix} \right) \tag{5.4}$$

The state space representation of the Kalman filter consists of the state space representation of the FEM-model found in equation 3.2 and the corrective term, $K_c = (y - (D\ 0)(\hat{x}\ \dot{\hat{x}})^T)$. The original FEM-model describes the system with large and sparse matrices as mentioned in 3.1. Inversion of the M-matrix generates a full matrix causing memory allocation error when trying to simulate. More consequences of the full M-inverse are that distribution of the originally sparse matrices is not straightforward.

5.2.1.1 Distribution

An approach to overcome the distribution problem caused by the full inverse of M is needed. Since M is sparse, a distributed approximation of its inverse can be done through introduction of an additional state variable, p. This p is introduced to approximate the second derivative of x without having to use a full inverse of the M-matrix. The second derivative approximation is:

$$\begin{aligned} p &= \ddot{x} \\ \dot{p} &= -g(Mp + C\dot{x} + Kx - F) \end{aligned} \tag{5.5}$$

If g is chosen large, $\dot{p}$ will converge to zero very fast. When $\dot{p}$ approaches zero, $Mp + C\dot{x} + Kx - F$ also approaches zero. According to equation 3.1, $M\ddot{x} + C\dot{x} + Kx - F = 0$. Thus p approaches $\ddot{x}$ when $\dot{p}$ approaches zero and

can serve as an approximation of the second derivative of x. The full system in state space with this approximation follows:

$$\begin{pmatrix} \dot{x} \\ \ddot{x} \\ \dot{p} \end{pmatrix} = \begin{pmatrix} 0 & I & 0 \\ 0 & 0 & I \\ -gK & -gC & -gM \end{pmatrix} \begin{pmatrix} x \\ \dot{x} \\ p \end{pmatrix} + \begin{pmatrix} 0 \\ 0 \\ gF \end{pmatrix} \tag{5.6}$$

This leaves a distributed system with sparse matrices. There are however problems with this approach. As mentioned, the full FEM-matrices, which are very large, are used. All states in the model have to be estimated to extract the estimations of the interesting 840 states used in the feedback (420 actuator position states and equally many actuator velocity states). More accurately 17343 states need to be estimated to obtain the required 840 estimates. The number of estimations needed is determined by the number of dofs in the full FEM-model (11562), multiplied by three because of the size of the state space model, and divided by two since z-translation do only depend on itself and x- and y-rotation. The estimation of the not required states is a time consuming and inefficient task that limits the sample frequency. The second problem is that of choosing the variable g. The difficulty lies in to make the system stable, while keeping it a good approximation to the real system. This was not accomplished. The structural damping of the system is very low, leading to instability when approximating the acceleration for almost all choices of g. By increasing the structural damping in the model, a stable system for some choices of g can be obtained. This choice of structural damping, however, does not represent the damping of the real system. Preceding arguments suggests that a model reduction is needed for the Kalman filter to be feasible.

5.2.2 Kalman filtering using a reduced model

Numerous reduction methods are discussed in chapter 3.2. The dynamic reduction method, see chapter 3.2.3 for further details, is used in the continuation because it is fairly rapidly computed and accurate enough. When using this reduced model in the observer, accurate results are obtained. The observer is described by equation 5.4, with the reduced matrices as system matrices. When using dynamic condensation master and slave states must be chosen. In this case the interesting z-translation for the actuators and sensors are chosen as master states. This results in reduced system matrices that are 1224×1224. Both the reduced system matrices and the M-inverse matrix are full. Hence the distribution problem is still not solved. An accurate Kalman filter is rather easily obtained. The difficulty is the distribution of the Kalman filter, which is addressed in the next section.

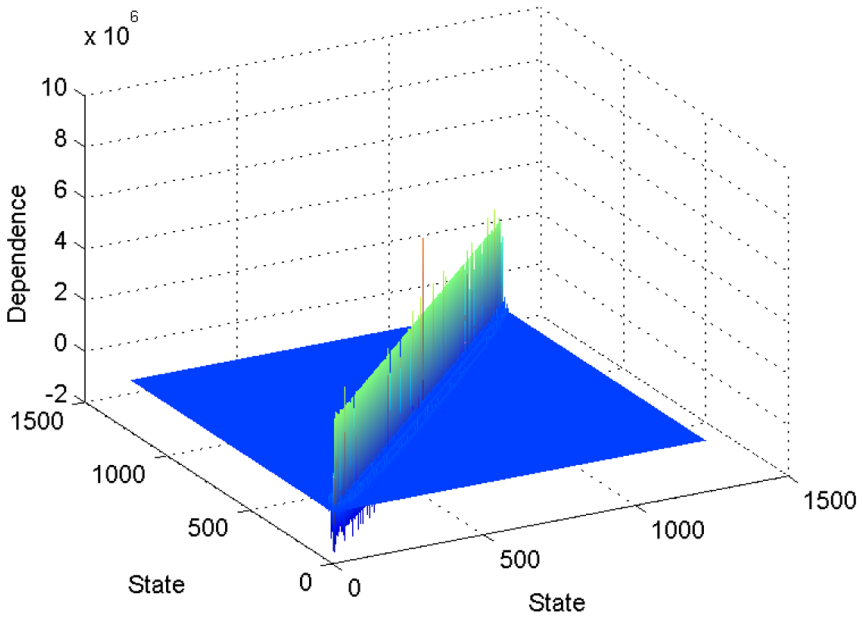

Figure 5.2: The figure shows a surface plot of the reduced stiffness matrix. As seen, far away states do not influence much. Altogether the far away states do, however, influence too much to be neglected.

5.2.2.1 Distribution

Physical considerations might imply that states spatially far away from the interesting state are of negligible importance, implying that the influence from these can be approximated to be zero. When examining the system matrices conclusions about the influence of far away states can be drawn to be small. Figure 5.2 shows a surface plot of the stiffness matrix of the reduced model. However, not only state dependencies need to be addressed. In order to create a distributed observer, far away inputs need to have negligible influence as well. The input matrix has similar structure as the stiffness matrix, saying that forces applied far away seem to have a negligible influence. Distribution of the Kalman filter might then be done through a dependence truncation of the system matrices. States and forces that influence less than a threshold of 0.1% upon a state will be approximated to not influence at all. This however has shown to be a too inaccurate approximation since there are too many states that have a small interaction that is neglected. Altogether this leads to a large dependence. If the influence threshold is reduced, the distribution areas become too large, leading to an unfeasible distribution.

Another distribution method would be to introduce a distributed Kalman fil-

ter. There is much literature[1] covering distribution of a Kalman filter with loops in the communication topology. Distribution of the Kalman filter used in this case will lead to extensive calculations. The reason is that every calculation unit includes the reduced model with estimates of all states in the Kalman filter model. Most of these states are not used as shown in the following example. There are 420 actuator and hence 420 calculation units distributed over the mirror. The Kalman filter system matrix seen in equation 5.4 is 2448×2448 which says that the state vector to be estimated contains 2448 states. Altogether this results in 420×2448=1028160 state estimates being performed at every update. The task for every calculation unit is to estimate position and velocity states for its associated actuator. Altogether 840 state estimates is needed for the feedback, that is the position and velocity for the 420 actuators. As seen, a distributed Kalman filter of this type is not recommendable because of the heavy calculation burden.

5.2.3 Kalman filtering using distributed local models

Previous sections say that a Kalman filter using the complete mirror model is hard to distribute over many calculation units. This suggests introduction of many small local Kalman filters that each estimate the states of one actuator. Every actuator is provided a unique local Kalman filter. Altogether these local Kalman filters estimate all actuator states. Figure 5.3 shows the local model in the Kalman filter. As seen, the center actuator depends only on the surrounding sensors and actuators within two actuator rings. Dynamic condensation, see 3.2.3, is used to derive the small local models needed for these Kalman filters. States associated with the actuators and sensors in the local model are chosen as master states in the reduction process. The mass and stiffness matrices are as usual rearranged in master and slave states:

$$\begin{pmatrix} M_{mm} & M_{ms} \\ M_{sm} & M_{ss} \end{pmatrix} \begin{pmatrix} \ddot{x}_m \\ \ddot{x}_s \end{pmatrix} + \begin{pmatrix} K_{mm} & K_{ms} \\ K_{sm} & K_{ss} \end{pmatrix} \begin{pmatrix} x_m \\ x_s \end{pmatrix} = \begin{pmatrix} F_1 \\ F_2 \end{pmatrix} \tag{5.7}$$

F_1 contains the forces applied inside the local model. An approximation has to be made to be able to implement these local models distributed. Forces outside the local model must be approximated to not directly affect the center of the model. In the equation this correspond to F_2 being zero. Dynamic condensation is applied to obtain the local model. The full system is described by the following equation with M, C and K rearranged as in equation 5.7:

$$M\ddot{x} + C\dot{x} + Kx = (F_1\ 0)^T \tag{5.8}$$

[1] See [3] for an example of a distributed Kalman filter.

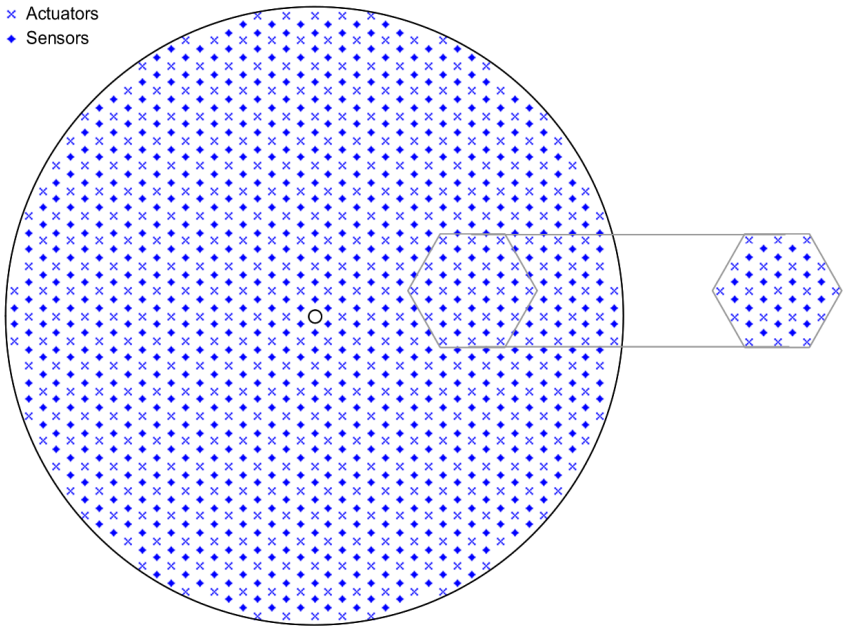

Figure 5.3: The left figure shows the deformable mirror as in figure 2.1. The right figure shows how the local models are chosen with one center actuator and all sensors and actuators within two actuator rings.

This equation is transformed by the transformation matrix T used in dynamic condensation, see chapter 3.2.3 for details:

$$T = \begin{pmatrix} I \\ -\left(K_{ss} - \omega^2 M_{ss}\right)^{-1} \left(K_{sm} - \omega^2 M_{sm}\right) \end{pmatrix} \tag{5.9}$$

The transformed model contains only the master states which says that a local model is obtained:

$$T^T M T \ddot{x}_m + T^T C T \dot{x}_m + T^T K T x_m = F_1 \tag{5.10}$$

New mass, damping and stiffness matrices are obtained that describe the local behavior, $T^T M T = M_r$, $T^T C T = C_r$, $T^T K T = K_r$. To use this model in a Kalman filter a state space representation is needed. The Kalman filter equation is:

$$\begin{pmatrix} \dot{\hat{x}}_m \\ \ddot{\hat{x}}_m \end{pmatrix} = \begin{pmatrix} 0 & I \\ -M_r^{-1} K_r & -M_r^{-1} C_r \end{pmatrix} \begin{pmatrix} \hat{x}_m \\ \dot{\hat{x}}_m \end{pmatrix} + \begin{pmatrix} 0 \\ M_r^{-1} \end{pmatrix} F_1 + K_c \left(y - D \begin{pmatrix} \hat{x}_m \\ \dot{\hat{x}}_m \end{pmatrix} \right) \tag{5.11}$$

The task for every local Kalman filter is, besides to estimate the states of the center actuator, also to estimate the states for one, two or three of its surrounding sensors.

Every actuator position will be the center in a local Kalman filter. This results in 420 different Kalman filters. The Kalman filters need accurate information from neighboring states and forces to estimate their states. These surrounding states are accurately estimated by other Kalman filters. The required state estimations are therefore provided by the surrounding Kalman filters.

The local models have in simulations shown to estimate the states accurately, both dynamically and statically, when fed with actual sensor and actuator state information. When the state estimates, on the contrary, originate from the other Kalman filters, as is planned for this observer, problems occur. Dynamically the observer behaves correctly, but when the mirror is static a state wind up in the estimation occur.

5.2.3.1 Problem - Sharing estimates

A scenario that reveals the cause of the wind up problem is described here. Denote an actuator A, anywhere on the mirror surface. One position and one velocity state is associated with this actuator, as well as all the other actuators. The states are estimated by the local Kalman filter and sent to the neighboring Kalman filters in order for them to update their states. Denote one of A:s neighboring Kalman filters B and assume that the mirror is static. B uses state and force information not used by A when estimating its states, since their respective local models are not the same. The state estimate originating from A might be slightly wrong in order for the state estimates in B to stay static. When the states in B have been updated, they are sent to all its neighbors, including to A. This will result in a slight change of state estimates also in A. The procedure is repeated between all Kalman filters, leading to a drift in the estimates. These loops, that cause the drift in the state estimates, exist all over the mirror surface between all shared estimates. This problem is needed to be solved for the distributed observer to function.

An approach to solving the drift problem is to share and to update the models using measurements instead of estimates. This approach need new local models where state estimates depend on sensor measurements and applied forces only.

5.2.3.2 Solution - Sharing measurements

As mentioned, new models have to be derived in order for estimates to depend on measured values only. Previously the local models contained actuator and sensor states in a surrounding area, see figure 5.3. This approach required actuator state information, that was estimated by other models. The fact that

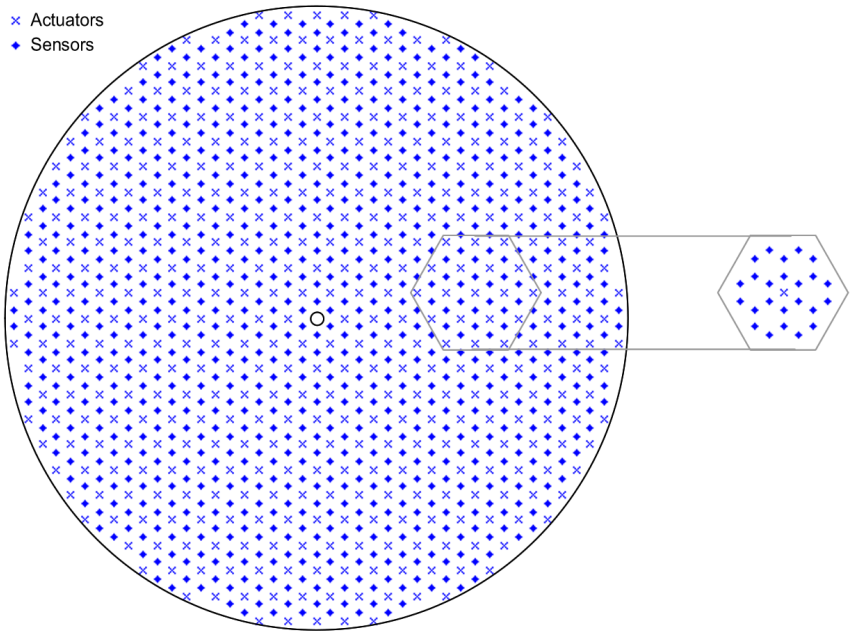

Figure 5.4: The left figure shows the deformable mirror as in figure 2.1. The right figure shows how the local models are chosen with one center actuator and all sensors within two actuator rings. The difference from the local model in 5.3 is that actuator states are not present in this model. To account for the forces applied at those actuators, their impacts are transformed into virtual forces at the sensor locations.

estimates was shared resulted in drift of state estimations. To overcome this problem, new models that depend on surrounding sensor states only, have been derived. The new local model is shown in figure 5.4. Here measurements and differentiated measurements can be directly applied when estimating the center actuator states. This solves the problem of estimation drift since measurements are shared instead of estimates. One issue concerning actuator forces remains however. In the previous local model, actuator states and the forces acting upon them, were included in the model. These forces do still directly affect the behavior of the center actuator states. Hence it is necessary for those forces to be accounted for in the new local models. The applied forces can actually be transformed to virtual forces at the surrounding sensors locations in the local model. This is done through dynamic condensation, chapter 3.2.3. The mass and stiffness matrices are as usual rearranged with the states in figure 5.4 chosen as master states:

$$\begin{pmatrix} M_{mm} & M_{ms} \\ M_{sm} & M_{ss} \end{pmatrix} \begin{pmatrix} \ddot{x}_m \\ \ddot{x}_s \end{pmatrix} + \begin{pmatrix} K_{mm} & K_{ms} \\ K_{sm} & K_{ss} \end{pmatrix} \begin{pmatrix} x_m \\ x_s \end{pmatrix} = \begin{pmatrix} F_1 \\ F_2 \end{pmatrix} \tag{5.12}$$

F_1 contains forces applied to the master states. The only master state that is an actuator, is the center actuator who's states are being estimated. Accordingly F_1 do only contain that force. F_2 contains all forces except the center actuator force. The forces applied outside the previously used local model is in F_2 approximated to be zero. The reason is to maintain the distribution. The remaining forces applied at actuator locations in the previous local model are here contained in F_2. The transformation matrix for dynamic condensation, see 3.9, is:

$$T = \begin{pmatrix} I \\ -\left(K_{ss} - \omega^2 M_{ss}\right)^{-1}\left(K_{sm} - \omega^2 M_{sm}\right) \end{pmatrix} \tag{5.13}$$

This is applied to the system:

$$M\ddot{x} + C\dot{x} + Kx = (F_1 \; F_2)^T \tag{5.14}$$

Leading to:

$$T^T M T\ddot{x}_m + T^T C T\dot{x}_m + T^T K T x_m = T^T (F_1 \; F_2)^T \tag{5.15}$$

x_m are the master states, that is, the states in the local model. $T^T M T = M_r$, $T^T C T = C_r$ and $T^T K T = K_r$ are the reduced mass, damping and stiffness matrices for this local model. These system matrices are always square and the size is the same as the number of master states chosen, that is 25 according to figure 5.4. This can be compared to the original mass, M, damping, C and stiffness, K, matrices that are 11562x11562. The transformation matrix does not only transform the system matrices to reduce the number of states needed, but does also transform force impact points. The right hand side of equation 5.15 can be written as:

$$T^T (F_1 \; F_2)^T = F_1 - (K_{ss} - \omega^2 M_{ss})^{-1}(K_{sm} - \omega^2 M_{sm}) F_2 \tag{5.16}$$

F_1 and F_2 are described above. As seen the force in F_1 acts directly on its corresponding state. The forces in F_2 are transformed to virtual forces applied at the master states. This force transformation is crucial to keep the estimation of the center actuator states accurate.

The local model in 5.15 is in a form not suitable for implementation in an observer. The equation can be written as:

$$M_r\ddot{x}_m + C_r\dot{x}_m + K_r x_m = F_r \tag{5.17}$$

A state space representation of the model is:

$$\begin{pmatrix} \dot{x}_m \\ \ddot{x}_m \end{pmatrix} = \begin{pmatrix} 0 & I \\ -M_r^{-1}K_r & -M_r^{-1}C_r \end{pmatrix} \begin{pmatrix} x_m \\ \dot{x}_m \end{pmatrix} + \begin{pmatrix} 0 \\ M_r^{-1} \end{pmatrix} F_r \tag{5.18}$$

or shorter,

$$\begin{pmatrix} \dot{x}_m \\ \ddot{x}_m \end{pmatrix} = A \begin{pmatrix} x_m \\ \dot{x}_m \end{pmatrix} + BF_r \tag{5.19}$$

The model needs to be discretized before realization in hardware. The discrete state space model is:

$$\begin{pmatrix} x(k+1) \\ \dot{x}(k+1) \end{pmatrix} = \Phi \begin{pmatrix} x(k) \\ \dot{x}(k) \end{pmatrix} + \Gamma F_r \tag{5.20}$$

where

$$\Phi = e^{Ah} \tag{5.21}$$

$$\Gamma = B \int_0^h e^{As}\, ds \tag{5.22}$$

As discussed, state measurements instead of state estimates are used in these local observers. The discrete model in equation 5.20 is placed in a observer and the observer equation becomes:

$$\begin{pmatrix} \widehat{x}_s(k+1) \\ \widehat{x}_a(k+1) \\ \dot{\widehat{x}}_s(k+1) \\ \dot{\widehat{x}}_a(k+1) \end{pmatrix} = \Phi \begin{pmatrix} y(k) \\ \widehat{x}_a(k) \\ \dot{y}(k) \\ \dot{\widehat{x}}_a(k) \end{pmatrix} + \Gamma F_r \tag{5.23}$$

$\widehat{x}_s$ and $\dot{\widehat{x}}_s$ denote sensor estimates. These estimates are not used. $\widehat{x}_a$ and $\dot{\widehat{x}}_a$ denote the center actuator estimates. These estimates are required for the state feedback and placed in the output from the observer. $y(k)$ in the equation say that sensor measurements instead of sensor estimates are used in the observer. This observer is not a Kalman filter and will be denoted as local observer in the continuation. Actually the actuator estimates consist of weighted sensor measurements from the local model from the startup of the observer until present time.

The idea of sharing measurements instead of estimates has eliminated the drift problem in the state estimates. The full distributed observer is obtained by implementing the local observers with their uniquely derived local models at every actuator location on the mirror.

5.2.3.3 Realization

The full observer consists of 420 unique discrete local observers described in equation 5.23. Every local observer is implemented in its own calculation unit, that is situated above their respective center actuator. This leads to 420 different calculation units distributed over the mirror surface. Altogether the

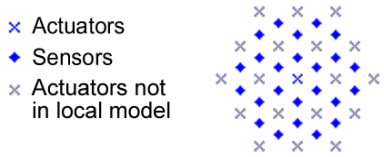

Figure 5.5: The figure shows a local model as in figure 5.4. The forces applied at the grey crosses are transformed to virtual forces at sensor locations. Every actuator has a calculation unit with a observer associated to itself. The closest neighbors of all sensors are a calculation unit within the figure. This implies that the communication of estimated states and applied forces need only to take place between the grey crosses and the center blue cross.

local observers estimate the actuator states required for the feedback. As mentioned, the local observers need state information from its surrounding sensors and force information from its surrounding actuators. The sensor signals will be differentiated to obtain the derivative information. Thus the sensor signals need to be low-pass filtered to increase the Signal to Noise-ratio in the differentiations. To minimize the number of low-pass filters needed, every calculation unit is assigned to collect data from one, two or three directly surrounding sensors and to low-pass filter their signals. The one, two or three sensors are chosen on beforehand for all sensors to be low-pass filtered by neighboring calculation units. These low-pass filtered signals are then sent to neighboring calculation units that need the information to update its estimates.

The area over which state and force information needs to be shared, is determined by the local models. Forces applied at actuators locations in the local model in figure 5.3, are transformed to virtual sensor forces. Those forces are therefore needed to update the estimates the local observers. The area of the required applied forces can be described as two actuator rings around the center actuator. Information about those forces are needed to be sent to the local observer at the center actuator. All sensor measurements needed, originate from sensors within this area. Thus one of the calculation units within the two actuator ring area, will low-pass filter the sensor signals in the model. This sensor state information will also be sent to the local observer at the center actuator. The communication area is hence not increased by the sensor state communications. This is exemplified in figure 5.5.

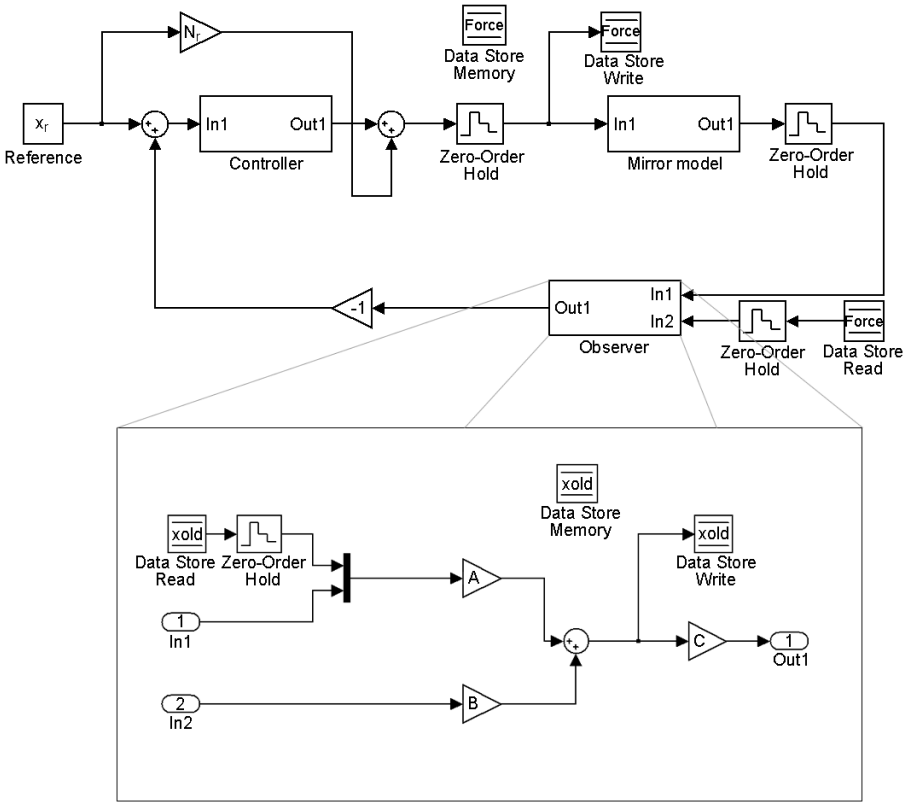

Figure 5.6: The figure shows the Simulink model of the system with the observer. The subsystems ”Mirror model” and ”Controller” are shown in figure 3.5 and 4.1 respectively. The local observers are discretized and assembled to one system representation in ”Observer”.

5.3 Simulation

Simulation of the full control system is, as before, performed in Simulink. The simulation routing is shown in figure 5.6. The control system consists of the observer and the 420 state feedback PD controllers. The observer actually consists of 420 small observers that each estimate the states of their respective center actuator. The A-matrix in the figure is an assembly of all the local discrete observers. A discrete local observer is described in equation 5.23. The lines associated with the center actuator state estimates for each local model are extracted from the Φ matrix in the local observer and placed in the A-matrix. The same holds for the B matrix with the difference that the interesting lines are taken from the Γ matrix instead. The C matrix passes the, for the state feedback, interesting state estimates through. This way the distributed observer, consisting of many small local observers, can be simulated in one system representation.

Chapter 6

Control System Evaluation

6.1 Proposed control system

To control this mirror, with its sensor and actuator configuration, a state feedback controller and an observer is needed. The proposed state feedback controller is a SISO controller of PD type. All 420 actuators are controlled using the same controller in order to minimize cross coupling effects. The SISO controller is described in section 4.2.1. These controllers need position and velocity information for the mirror at actuator locations. Since no sensors are available there, these states have to be estimated by and observer. The proposed observer consists of as many local observers as there are actuators, namely 420. These observers are based on local models that include the desired actuator states and surrounding sensor states. The sensor position states are measured, and their velocity states are obtained through differentiation of the position signals. The proposed observer is more accurately described in section 5.2.3 from the subsection Sharing measurements and onward.

In the subsequent sections of this chapter robustness and performance of the control system will be evaluated. For these tests to have relevance, the controllers must be tuned. As mentioned the PD controllers all over the mirror are chosen equal. The control parameters are chosen to obtain required performance but still to have satisfactory robustness to disturbances. Tests have shown that a proportional gain, N, of 0.15 N/μm and a derivative gain, L, of 75 Ns/m is a good tradeoff. The derivative part creates well damped step responses to prevent oscillations and large overshoots. The feed forward term N_r is calculated to eliminate static errors.

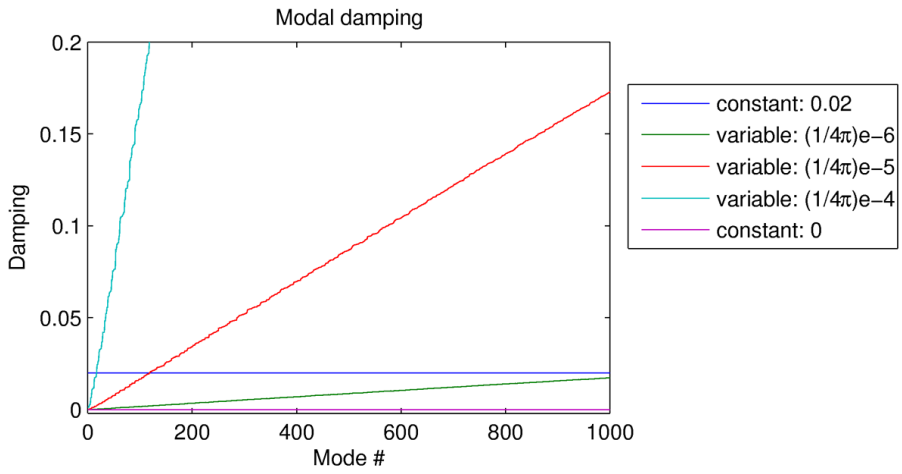

Figure 6.1: The figure shows modal damping properties of different mirror models.

6.2 Sampling frequency

Throughout this thesis rapidly sampled or continuous sensor measurements have been assumed. This is not feasible when realizing the control system in hardware. A rule of thumb is to use at least ten to twenty times as high sampling frequency as the desired closed loop bandwidth. The closed loop bandwidth is around 1 kHz leading to a sampling frequency of at least 10 to 20 kHz according to the rule of thumb. Because of the many resonance frequencies inside the closed loop bandwidth, a sampling frequency of 20 kHz was decided upon.

6.3 Robustness to modeling errors

It is not probable that the damping properties of the observer and the actual mirror will fit. Hence robustness to errors in the observer damping must be evaluated.

The derived controller uses a derivative part for damping purposes. The damping force is proportional to the velocity of the actuator at a given time. If the damping properties of the observer model are false, a damping force of opposite sign might occur. This might lead to instability. Hence the robustness to damping matrix errors in the controller, depends on the derivative gain. Less derivative gain leads to a worse performing controller. As always this is a balance between performance and robustness.

Mirror damping: $f\times(1/4\pi)\times10^{-6}$

D-gain, L	**Stability**	**RMS value**
0	yes	2.5μm
30	yes	890nm
75	yes	220nm
125	no	
200	no	

Mirror damping: $f\times(1/4\pi)\times10^{-5}$

D-gain, L	**Stability**	**RMS value**
0	yes	2.5μm
30	yes	890nm
75	yes	220nm
125	yes	420nm
200	yes	890nm

Mirror damping: $f\times(1/4\pi)\times10^{-4}$

D-gain, L	**Stability**	**RMS value**
0	yes	2.4μm
30	yes	860nm
75	yes	220nm
125	yes	420nm
200	yes	890nm

Mirror damping: Zero

D-gain, L	**Stability**	**RMS value**
0	yes	2.5μm
30	yes	890nm
75	yes	220nm
125	no	
200	no	

Mirror damping: Constant, 0.02

D-gain, L	**Stability**	**RMS value**
0	yes	2.5μm
30	yes	880nm
75	yes	220nm
125	no	
200	no	

Table 6.1: The table presents robustness to modeling errors. The dependence on derivative gain (D-gain) is also shown. A, in this case relative, performance indicator, RMS, is also presented. The f denotes modal frequency in Hz.

In these robustness tests the mirror model will be assigned different modal damping whereas the observer model will have the same damping properties throughout the test. Structural damping is usually described as a modal damping that is constant, or a modal damping that is dependent of the eigenfrequency. The different damping properties used in the tests are plotted in figure 6.1. The observer damping properties has been chosen to be the eigenfrequency variable, that is the eigenfrequency multiplied with a factor, here $(1/4\pi)\times10^{-4}$. This damping is higher than the probable mirror damping, leading to a more damped observer than the actual mirror. This choice will be justified later. The test is performed to evaluate not only the robustness to different mirror damping properties, but also to see how the derivative gain in the controllers affect stability. Stability is checked for all test cases and the RMS value for deformation deviation is calculated. Thus both robustness and a performance can be evaluated. The tests are made within a short time frame in where large steps on all actuators are applied. The RMS values presented are because of the transients much larger than corresponding RMS values when running the controller for a longer period of time. The RMS values can however be compared to each other to evaluate performance differences. Test results are printed in table 6.1.

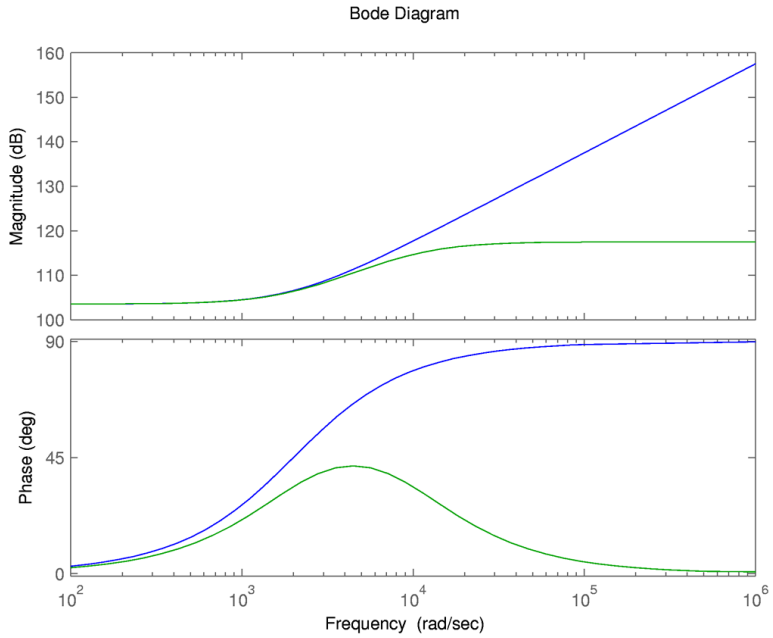

Figure 6.2: The blue line shows frequency response for the PD-controller without low-pass filtering of sensor signals. The green line shows frequency response for the PD-controller when sensor signals are low-pass filtered.

The table reveals that the higher the derivative gain is, the less robust the control system is to errors in the damping matrix. A high derivative gain is needed to obtain required performance. $L = 75$, however, manages to keep the system stable in all cases, but it is very oscillating and close to instability. Too high derivative gain leads to an over damped system which is revealed in the RMS-value of $L = 125$ and 200. When examining the instability frequency closer, it is revealed that the high order modes cause the instability. The reason is that the derivative part of the controller amplifies high frequency modes much. As mentioned earlier, high frequent modes can be seen as noise to the system. A low-pass filter can be introduced to suppress the high frequency modes that cause instability. The low pass filter should suppress the high order modes, but still not introduce too much phase lag to the other modes. The effect of the low-pass filtering can be viewed in a bode plot that compares the original SISO controller with the one where the sensor signals are being low-pass filtered before. This is done in figure 6.2, where the low-pass filter is chosen to be $1/(s/10000 + 1)$. A consequence of the low-pass filter and the resulting phase lag is that the controller performs worse. The choice of using observer damping that is higher then the probable mirror damping, is justified by the introduction of the low-pass filter. Information about high frequency oscilla-

Mirror damping: $f\times(1/4\pi)\times10^{-6}$

D-gain, L	**Stability**	**RMS value**
0	no	
30	yes	1.3μm
75	yes	290nm
125	yes	350nm
200	yes	820nm

Mirror damping: $f\times(1/4\pi)\times10^{-5}$

D-gain, L	**Stability**	**RMS value**
0	no	
30	yes	1.3μm
75	yes	280nm
125	yes	340nm
200	yes	820nm

Mirror damping: $f\times(1/4\pi)\times10^{-4}$

D-gain, L	**Stability**	**RMS value**
0	no	
30	yes	1.3μm
75	yes	270nm
125	yes	340nm
200	yes	820nm

Mirror damping: Zero

D-gain, L	**Stability**	**RMS value**
0	no	
30	yes	1.3μm
75	yes	290nm
125	yes	340nm
200	yes	820nm

Mirror damping: Constant, 0.02

D-gain, L	**Stability**	**RMS value**
0	no	
30	yes	1.3μm
75	yes	280nm
125	yes	350nm
200	yes	820nm

Table 6.2: The table presents robustness to modeling errors when sensor signals are low-pass filtered before entering the observer. The dependence on derivative gain is also shown. A, in this case relative, performance indicator, RMS, is also presented. The f denotes modal frequency in Hz.

tions is canceled by the low-pass filter. Thus it is inappropriate to introduce high frequency oscillations by using a poorly damped observer since these oscillations will not correspond to actual oscillations in the mirror. The previous robustness tests are again undertaken with the difference that sensor signals are being low-pass filtered before entering the observer. The results are presented in table 6.2.

The table reveals that other choices of damping matrices and derivative gains do cause instability. The low-pass filter has eliminated the cause of high frequency instability, but has instead introduced low frequency instability when no derivative gain is used. This instability occurs due to the phase lag introduced by the low-pass filter. If the controller uses derivative gain, the phase is increased in the crucial frequency range, hence leading to stability. The derivative gain can however not be increased too much. This would again lead to a too large high frequency amplification and the problem with high frequency instability would be reintroduced. The robustness to damping matrix errors has been made fairly large after the introduction of a low-pass filter.

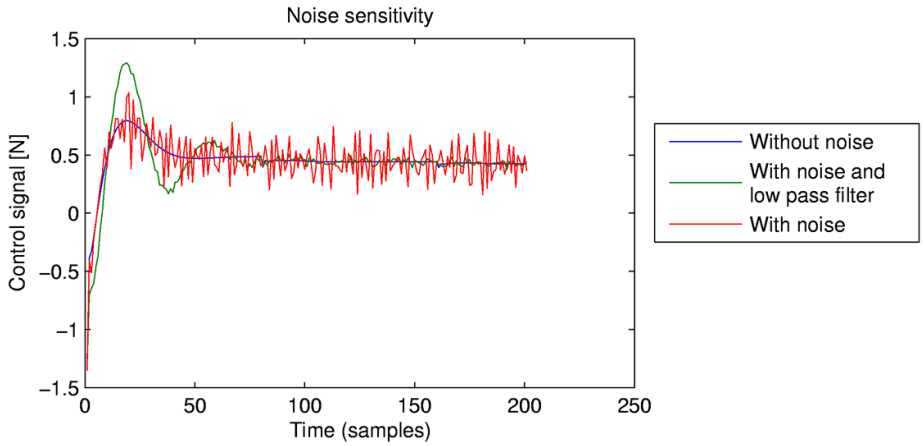

Figure 6.3: The figure shows the control signal for one actuator under different measurement noise circumstances.

6.4 Robustness to sensor noise

So far sensor measurements without noise have been used in simulations. The sensors are specified to have noise less than 50 nm. White independent noise with zero mean is inserted in the simulation environment to simulate the expected noise in the actual sensors. When simulating with sensor noise and the suggested control parameters, without a low-pass filter, the noise does not affect the output significantly. Hence the controller is adequately robust to sensor noise of this specified magnitude.

The sensor velocity is, as mentioned, estimated through differentiation of the sensor signal. When the sensor signals are affected by noise, the sensor velocity estimates will be very choppy. This will lead to choppy control signals as well. In the previous section a low-pass filter was introduced to ensure high frequency stability. This low-pass filter is also needed for measurement noise to be suppressed to keep the Signal to Noise Ratio (SNR) acceptable after differentiation. Figure 6.3 shows control signals to one of the actuators when using realistic references with an initial step to all actuators. The figure shows the difference between the control signals when the sensor signals are low-pass filtered and when they are not. It does also, as comparison, show the control signal when the sensor signals are not low-pass filtered and there is no noise present. The control signal when using a low-pass filter has larger overshoot due to the phase lag. Since the sensors that will be used to measure mirror deflections are specified to have very little noise, this will not constitute a major problem.

6.5 Robustness to time delays

Robustness to time delays in the communication of measurements and applied forces is crucial to the control system. The proposed observer need information from sensor states and actuator forces that are located within two actuator rings from the actuator whose states are being estimated, see figure 5.5. The communication of measured states and applied forces cannot be performed without time delays. The robustness with respect to these delays has to be examined. The robustness tests will be undertaken using the different mirror model damping properties used in table 6.1. The observer damping is also the same as in table 6.1, namely $(1/4\pi)\times10^{-4}$ times the eigenfrequency. Table 6.3 shows the maximum delay in complete samples before instability occurs for different damping properties.

Observer damping: Eigen frequency $\times$ $(1/4\pi)\times10^{-4}$

Modal mirror damping	**Nbr of samples delay**
Constant, 0.02	1
Eigen frequency $\times$ $(1/4\pi)\times10^{-6}$	1
Eigen frequency $\times$ $(1/4\pi)\times10^{-5}$	2
Eigen frequency $\times$ $(1/4\pi)\times10^{-4}$	5

Table 6.3: The table presents robustness to time delays for different mirror dampings.

As seen, the robustness is largely dependent on the actual mirror damping. The less the mirror damping is, the less robust to time delays the system becomes. The delay causes high frequent instability for all cases except when the mirror damping is as high as the observer damping. Then a low frequency instability occurs because the high frequent modes are naturally damped out due to the higher damping. If low mirror damping diminishes the robustness to time delays, it might be advantageous to use a lower observer damping as well, to estimate the derivative more accurately. Simulations have, however, shown that lower observer damping leads to worse robustness. The reason is that sensor signals are low-pass filtered, hence information about high frequency modes do not reach the observer. Then, if the observer damping property is low, high frequency modes in the observer output are created by the observer itself and do not originate from the actual mirror. Then the controller acts upon invented high frequency derivatives which easily can excite high frequency modes. When instead using a higher observer damping, the high frequency modes that do not reach the observer, are not present in the observer output either. These high frequency modes are therefore left uncontrolled and will be damped by the natural mirror damping. This implies that

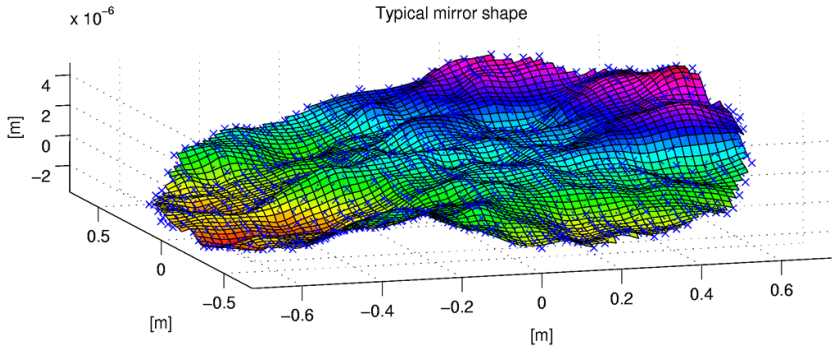

Figure 6.4: This is a typical shape of the mirror that compensates for atmospheric distortion.

the choice of a relatively high observer damping will lead to a more robust controller.

6.6 Performance evaluation

In section 2.1 performance specifications of the control system are stated. They concern the RMS value of deflection deviations, and closed loop bandwidth. The RMS value for reference to output deviation is specified to be below 80 nm for every actuator. To obtain realistic results of how the control law would perform when applied in a telescope, realistic reference signals are needed. They are generated through simulation of atmospheric disturbances. These atmospheric phase distortions are then transformed to path differences at actuator locations. It is these path differences that must be compensated for. They are therefore mapped to act as reference signals for the actuators. An example of references for the mirror at a certain time is shown in figure 6.4. To further make the simulation as realistic as possible, a delay of one sampling period is introduced. Also noise is inserted to the simulation. A constant modal damping of 0.02 is chosen for the mirror, The observer damping is chosen higher, namely $(1/4\pi)\times 10^{-4}$ times the eigenfrequency. Simulations over 0.8 seconds has been undertaken to evaluate the performance.

The reference tracking result of the simulation is for one of the actuators is found in figure 6.5. The accuracy in the reference tracking can be described by the RMS value for deflection deviations from the reference. The largest RMS value was 85.5nm and obtained at the outer edge of the mirror. The smallest RMS value was 13.4nm and obtained close to the fixed center. These RMS-values satisfy the specified requirements closely enough. Hence the performance of the controller is satisfying.

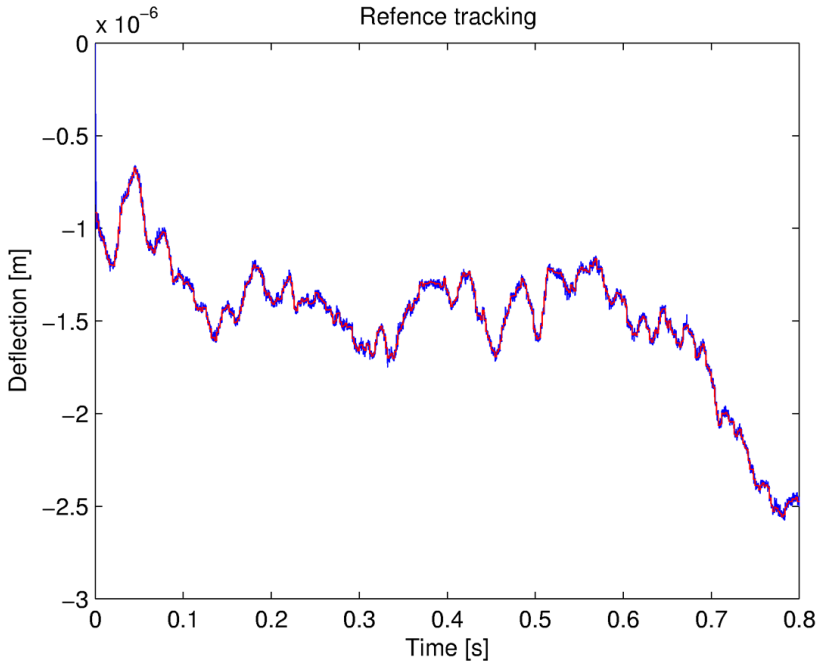

Figure 6.5: The figure shows reference tracking for one of the actuators. The red line is the reference signal and the blue line is the output. The RMS value for the reference tracking in this figure is 18.1nm.

To determine the bandwidth of the different control loops over the mirror a sine wave reference can be applied. The closed loop bandwidth is defined as the frequency where the actuator deflection follows the sine wave reference with an amplitude of -3 db (= 0.708) of the reference amplitude. The bandwidth for the different controllers is around 1 kHz, which well satisfy the requirements. The phase lag is around 50 degrees at the bandwidth frequency. Bode diagrams of the closed loops for the different actuators are plotted in figure 6.6.

6.7 Hardware requirements

Actuators and sensors have so far been treated as ideal. That is with a constant transfer function. Because of the sampling frequency of 20 kHz, they should operate close to an ideal actuator or sensor within this bandwidth. Further requirements on the hardware are due to communication speed and computational effort. The delay in communication of states and applied forces should be one sample length or less to not introduce too much phase lag. The proposed control strategy does also set a requirement regarding the speed at which states and applied forces need to be communicated.

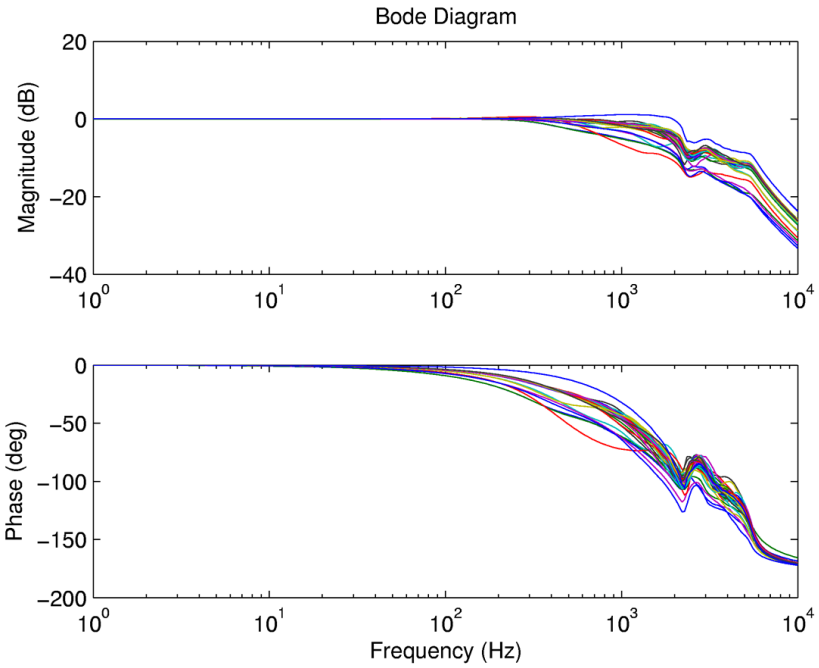

Figure 6.6: Closed loop Bode plots for all actuator to actuator transfer functions when fed with actual state information and controlled by the chosen PD-controllers. The modal mirror damping is here 0.02.

Assume that there are no delays in sensor measurements. Further assume that the communication is performed in single precision and that there is one calculation unit for every actuator position. Then, for every state and applied force that is to be sent to another calculation unit, 32 bit times 20 kHz equals 0.61 Mbit/s is required by the communication channel. One calculation unit is set to send the low-pass filtered position state of one, two or three surrounding sensors and the applied force upon the actuator to neighboring calculation units. This says that a maximum of four signals are being sent between two calculation units in one direction. This sets the minimum requirement of the speed to 0.61*4 = 2.5 Mbit/s. This communication has to be performed with full duplex since the estimates are shared in both directions. Then 5.0 Mbit/s will be sent through the communication channels. Altogether there are 420 calculation units each connected to between 9 and 18 neighboring calculation units. Altogether this requires 3417 communication channels with full duplex that interconnects the different calculation units. This results in an overall dataflow of 5.0 Mbit/s times 3417 communication channels = 16.6 Gbit/s. This communication burden will produce a lot of heat, setting requirements on the cooling capacity of the mirror setup.

6.8 Alternative hardware configuration

A way to extensively reduce control complexity is to let sensors and actuators be collocated. Then no observer is required and the communication of states and forces at a total of 16Mbit/s is no longer needed. This also eliminates the problem of delays due to the communication. Further the 3417 communication channels no longer needs to be mounted. The robustness to mirror modeling errors, especially robustness to errors in the chosen damping matrix, is greatly improved. To control the system where sensors and actuators are collocated, only PD controllers at every actuator location is needed.

A design with collocated sensors and actuators is more expensive due to requirements of higher manufacturing and mounting precision, than when sensors and actuators are not collocated. On the other hand, collocated sensors and actuators lead to an increased simplicity and decreased sensitivity to errors in the control system. These factors need to be compared and evaluated before a hardware setup is decided upon.

6.9 Simulation

The performance evaluation was performed in Simulink. Figure 6.7 shows the Simulink model of the realistic performance test. The Delay in the figure represents communication delays for forces and state estimates. The Differentiator differentiates the signals and passes both the incoming position signals and the differentiated signals on. The differentiation is performed in the following way:

$$\dot{x}(k) = \frac{x(k) - x(k-1)}{h} \tag{6.1}$$

where h is the sampling frequency. The low-pass filter is chosen to be $1/(s/10000+1)$, that is $y = 1/(s/10000+1)u$. A state space representation of the low-pass filter is:

$$\dot{x} = -10000x + 10000u \tag{6.2}$$

$$y = x \tag{6.3}$$

This state space model is discretized:

$$x(k+1) = 0.61x(k) + 0.39u(k) \tag{6.4}$$

$$y(k) = x(k) \tag{6.5}$$

This discrete state space model of the low-pass filter is placed in the Ad and Bd matrices respectively. One model for each sensor signal. The other blocks are described in the simulation section of their respective chapter.

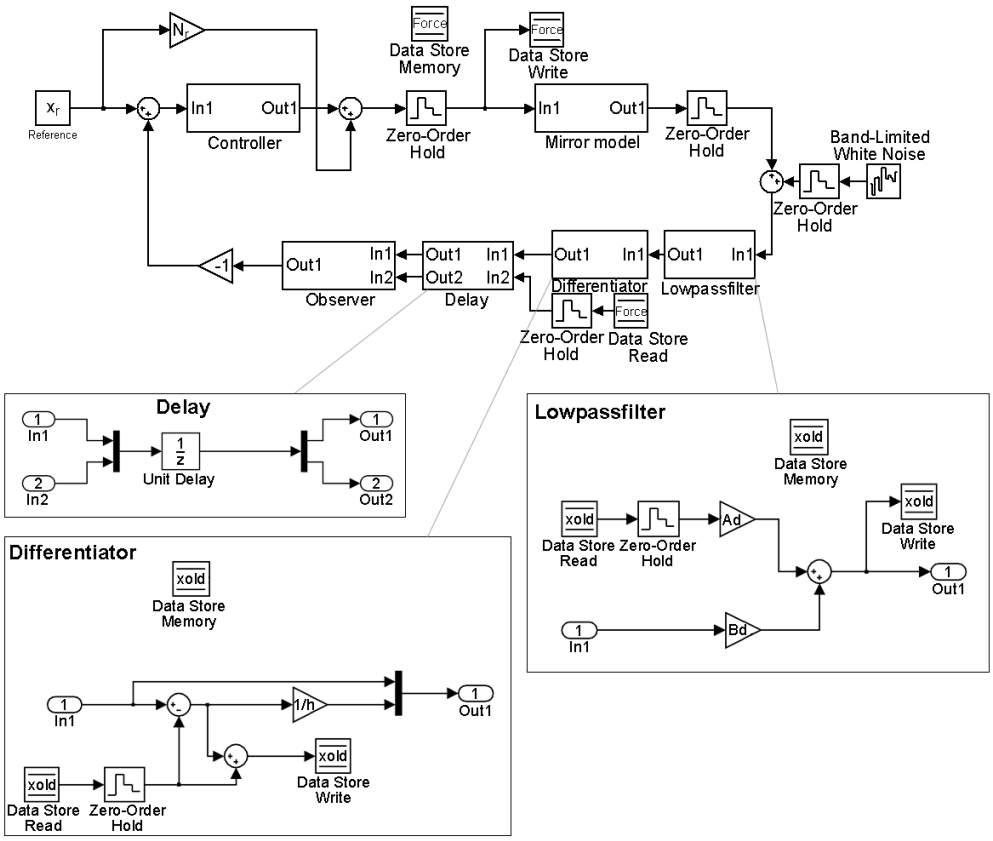

Figure 6.7: The figure shows the Simulink model used when simulating the realistic test. The subsystems ”Observer”, ”Mirror model” and Controller are shown in figures 5.6, 3.5 and 4.1 respectively.

Chapter 7

Conclusions

Controlling a large deformable mirror under hard performance specifications was certainly a challenge. The main difficulty originated in the fact that the sensors were not collocated with the actuators in the specified design. Since actuator state feedback control was desired, estimates of actuator states were required. To limit communication burdens, the observer that performs the estimations needed to be distributed. To find a distributed observer capable to perform these estimations accurately, was the main difficulty as well as the key to success in this project.

The derived distributed observer consists of many local observers, one for each actuator, that altogether estimate the required actuator states. The state estimations are, as mentioned, performed to supply state feedback controllers with state information. These state feedback controllers, that control the actuator forces, are of PD type. This control system satisfies the performance specifications and is adequately robust to modeling errors and time delays.

There are still uninvestigated matters needed to be addressed before the control system is ready to be implemented in hardware. These matters include the affect of having non-ideal actuators and sensors. Further, the sensor signals in this Master Thesis have been assumed to be exactly known. The proposed sensors, located at the back of the mirror, can however only measure variations in mirror behavior above approximately 20 Hz. Their signals do therefore not contain any information about their offsets from the nominal position. This low frequency and static information will be provided from the WFSs described in 1.4. These two sensor signals must be added somehow to obtain correct sensor measurements. These matters as well as hardware related matters need to be addressed before implementation. Anyway, adaptive optics on large deformable mirrors seems to be a solvable task and hopefully this contribution can be useful in the continuation.

Bibliography

[1] Large Binocular Telescope. URL: http://www.lbto.org/ (Accessed: Sep 10, 2006).

[2] Multiple Mirror Telescope. URL: http://cfa-www.harvard.edu/mmt/ (Accessed: Sep 10, 2006).

[3] P. Alriksson and A. Rantzer. Distributed Kalman Filtering Using Weighted Averaging. 2006.

[4] A. Riccardi et al. The adaptive secondary mirror for the 6.5 m conversion of the Multiple Mirror Telescope. Osservatorio Astrofisico di Arcetri et al., Firenze et al., Italy, 2001.

[5] A. Riccardi et al. Adaptive secondary mirrors for the Large Binocular Telescope. Osservatorio Astrofisico di Arcetri et al., Firenze et al., Italy, 2004.

[6] M.I. Friswell et al. The convergence of the iterated IRS method. *Journal of Sound and Vibration*, 1998.

[7] T. Andersen et al., editor. *Euro50 - A 50 m Adaptive Optics Telescope*. ISBN 91-631-4317-8. Lund Observatory, 2003.

[8] C. Felippa. Course material: Introduction to finite element methods - ASEN 5007. University of Colorado, Fall 2005. http://www.colorado.edu/engineering/CAS/courses.d/IFEM.d/Home.html (Accessed: Sep 10, 2006).

[9] C. Felippa. Course material: Advanced finite element methods - ASEN 5367. University of Colorado, Spring 2006. http://www.colorado.edu/engineering/CAS/courses.d/AFEM.d/Home.html (Accessed: Sep 10, 2006).

[10] W.K. Gawronski. *Dynamics and Control of Structures - A Modal Approach*. ISBN 91-631-4317-8. Springer, New York, 1998.

[11] J.W. Hardy. *Adaptive Optics for Astronomical Telescopes*. ISBN 0-19-509019-5. Oxford University Press, New York, 1998.

[12] R.J. Roark and W.C. Young. *Formulas for Stress and Strain*. ISBN 0-07-053031-9. McGraw-Hill, New York, fifth edition, 1975.